








Article

Effect of Textural Properties and Presence of Co-Cation on NH₃-SCR Activity of Cu-Exchanged ZSM-5

Magdalena Jabłońska ^{1,*}, Kinga Góra-Marek ², Miha Grilc ³, Paolo Cleto Bruzzese ⁴, David Poppitz ¹, Kamila Pyra ², Michael Liebau ¹, Andreas Pöppl ⁴, Blaž Likozar ³ and Roger Gläser ¹

¹ Institute of Chemical Technology, Universität Leipzig, Linnéstr. 3, 04103 Leipzig, Germany; david.poppitz@uni-leipzig.de (D.P.); michael.liebau@uni-leipzig.de (M.L.); roger.glaeser@uni-leipzig.de (R.G.)

² Faculty of Chemistry, Jagiellonian University in Kraków, Gronostajowa 2, 30-387 Kraków, Poland; kinga.gora-marek@uj.edu.pl (K.G.-M.); kamila.pyra@doctoral.uj.edu.pl (K.P.)

³ Department of Catalysis and Chemical Reaction Engineering, National Institute of Chemistry, Hajdrihova 19, 1001 Ljubljana, Slovenia; Miha.Grilc@ki.si (M.G.); blaz.likozar@ki.si (B.L.)

⁴ Felix Bloch Institute for Solid State Physics, Universität Leipzig, Linnéstr. 5, 04103 Leipzig, Germany; paolo.bruzzese@physik.uni-leipzig.de (P.C.B.); poepl@physik.uni-leipzig.de (A.P.)

* Correspondence: magdalena.jablonska@uni-leipzig.de

Abstract: Comparative studies over micro-/mesoporous Cu-containing zeolites ZSM-5 prepared by top-down treatment involving NaOH, TPAOH or mixture of NaOH/TPAOH (tetrapropylammonium hydroxide) were conducted. The results of the catalytic data revealed the highest activity of the Cu-ZSM-5 catalyst both in the absence and presence of water vapor. The physico-chemical characterization (diffuse reflectance UV-Vis (DR UV-Vis), Fourier transform infrared (FT-IR) spectroscopy, electron paramagnetic resonance (EPR) spectroscopy, temperature-programmed desorption of NO_x (TPD-NO_x), and microkinetic modeling) results indicated that the microporous structure of ZSM-5 effectively stabilized isolated Cu ion monomers. Besides the attempts targeted to the modification of the textural properties of the parent ZSM-5, in the next approach, we studied the effect of the co-presence of sodium and copper cations in the microporous H-ZSM-5. The presence of co-cation promoted the evolution of [Cu–O–Cu]²⁺ dimers that bind NO_x strongly with the desorption energy barrier of at least 80 kJ mol^{−1}. Water presence in the gas phase significantly decreases the rate of ammonia oxidation, while the reaction rates and activation energies of NH₃-SCR remain unaffected.

Keywords: zeolite ZSM-5; micro-/mesoporous zeolites; copper; co-cation; NH₃-SCR



Citation: Jabłońska, M.; Góra-Marek, K.; Grilc, M.; Bruzzese, P.C.; Poppitz, D.; Pyra, K.; Liebau, M.; Pöppl, A.; Likozar, B.; Gläser, R. Effect of Textural Properties and Presence of Co-Cation on NH₃-SCR Activity of Cu-Exchanged ZSM-5. *Catalysts* **2021**, *11*, 843. <https://doi.org/10.3390/catal11070843>

Academic Editor: Jose L. Hueso

Received: 14 June 2021

Accepted: 7 July 2021

Published: 13 July 2021

Publisher's Note: MDPI stays neutral with regard to jurisdictional claims in published maps and institutional affiliations.



Copyright: © 2021 by the authors. Licensee MDPI, Basel, Switzerland. This article is an open access article distributed under the terms and conditions of the Creative Commons Attribution (CC BY) license (<https://creativecommons.org/licenses/by/4.0/>).

1. Introduction

The selective catalytic reduction of NO_x with ammonia (NH₃-SCR) serves as one of the most efficient methods among the post-combustion technologies of NO_x emission control. Until now, different catalysts were investigated in NH₃-SCR, including Cu-ZSM-5, Cu-Y, Cu-Beta and Cu-SSZ-13, etc. [1]. The catalytic activity and N₂ selectivity of copper-containing zeolites are dependent on the topology of the zeolite, copper loading, and the nature and aggregation of introduced copper species [2]. The controlled deposition of copper species can be achieved by the modification of zeolite support, e.g., via the introduction of second porosity [3] and/or co-cation (e.g., Na, K, Ce, etc.) [4]. For example, Rutkowska et al. [3] investigated Cu-ZSM-5 with a micro-/mesoporous structure and found that a significantly higher amount of copper, ca., 2.5–4.1 wt % of Cu can be deposited in the micro-/mesoporous ZSM-5 versus 1.2 wt % of Cu deposited in ZSM-5 (*n*(Si)/*n*(Al) = 14). The higher content of easily reducible copper species of micro-/mesoporous Cu-ZSM-5 resulted in enhanced activity and N₂ selectivity during NH₃-SCR. Recently, Peng et al. [5] investigated micro-/mesoporous zeolite ZSM-5 prepared through a facile one-pot hydrothermal synthesis. The textural and acidic/redox properties of micro-/mesoporous Cu-ZSM-5 (1.98 wt % of Cu) were indicated as advantageous in NH₃-SCR

compared to Cu-ZSM-5 (2.01 wt % of Cu). The nature and aggregation state of copper species were also reported to be influenced by the presence of alkali metals. For example, Sultana et al. [4] have investigated Na-ZSM-5 ($n(\text{Si})/n(\text{Al}) = 14$, 4 wt % of Na_2O) and found that when the co-cation (Na^+) is present more copper species (3.5 wt %) could be introduced into ZSM-5 than when the H^+ is present (2.6 wt %). Consequently, the enhanced activity in NH_3 -SCR over Na-Cu-ZSM-5 was assigned to the concentration of Cu^+ species and easily reducible copper species present in this sample. Additionally, Gao et al. [6] investigated Cu-SSZ-13 ($n(\text{Si})/n(\text{Al}) = 6$), and they showed that when co-cation, i.e., Na^+ , K^+ , Li^+ , is present the amount of introduced copper species increased from 0.87 wt % for Cu-H-SSZ-13 to 0.94–0.98 wt % for Cu(Li,Na,K)-SSZ-13. The authors also revealed that the presence of certain amount of Na^+ (up to 1.78 wt %) (or other alkali and alkaline earth cations) is beneficial to both low-temperature NO_x conversion and hydrothermal stability of low-Cu loaded Cu-SSZ-13. These values (Na^+ content up to 1.7 wt % among 0.1–3.4 wt % of Na) was also confirmed in other studies over Na-Cu-SSZ-13 ($n(\text{Si})/n(\text{Al}) = 4$, 2.4–2.7 wt %) applied in NH_3 -SCR [7]. Delahay et al. [8] and Kieger et al. [9] have reported that the introduction of alkaline (Na^+) and lanthanide ions into faujasite (FAU, $n(\text{Si})/n(\text{Al}) = 2.55$) enhances the low-temperature NH_3 -SCR activity and N_2 selectivity of Cu-FAU. Occupation of the sodalite cages of FAU by sodium cations makes the copper sites more accessible to reagent molecules, thus increasing the activity and N_2 selectivity in NH_3 -SCR over Cu-FAU. Coq et al. [10] have reported the influence of H^+ , Na^+ and Ba^+ cations on the redox properties of Cu-FAU ($n(\text{Si})/n(\text{Al}) = 2.55$, 2.50–7.24 wt % of Cu) using operando DRIFTS studies. Especially, the presence of Ba^{2+} promoted the evolution of $[\text{Cu}-\text{O}-\text{Cu}]^{2+}$ dimers. The copper species (isolated Cu^{2+} and Cu^+ as well as $[\text{Cu}-\text{O}-\text{Cu}]^{2+}$) are reported to participate in NO_x reduction; only limited evidence was present to suggest such participation of active copper species.

As shown above, although a significant amount of studies are present over copper-based catalysts for NH_3 -SCR (mainly in the feed containing NH_3 , O_2 , NO balanced with inert gas and without H_2O), only limited number of studies focus on micro-/mesoporous Cu-ZSM-5 applied in NH_3 -SCR. Moreover, there is still a considerable gap in the fundamental understanding of the function of the active copper species over micro-/mesoporous Cu-ZSM-5 in NH_3 -SCR, especially in the presence of water vapor. Thus, this work aims to identify the nature of copper species present in Cu-ZSM-5 with a different texture (introduced mesoporosity) or co-cation, i.e., Na^+ . We applied a combination of spectroscopic (DR UV-Vis, EPR, FT-IR spectroscopy) and temperature-programmed methods (TPD- NO_x) to identify and quantify the nature of active centers on Cu-exchanged ZSM-5 in NH_3 -SCR (also in the presence of 5 vol.% of water vapor).

2. Results and Discussion

2.1. Structural and Textural Properties

Figure 1 shows the X-ray diffraction (XRD) patterns of H-ZSM-5 and Cu-exchanged ZSM-5. Powder X-ray diffraction patterns of the samples exhibit the diffraction peaks characteristic of MFI-type materials. The zeolite structure is preserved after the post-modification of H-ZSM-5 with an aqueous solution of NaOH, TPAOH or their mixture (NaOH/TPAOH), however, lowered crystallinity of Cu-exchanged zeolite was evidenced (Table 1). This also indicates that the ion-exchange treatment with ammonium ion and/or impregnation with copper (II) ion affected the structure of ZSM-5. Only in the case of Cu-Na-ZSM-5, the crystallinity reached 131%, mainly due to the ion-exchange of H-ZSM-5 with Na (increase to 134% for Na-ZSM-5). Otherwise, we observed the decrease in crystallinity to ca. 66% of K-Cu-ZSM-5 (results not shown). Thus, the crystallinity appears to depend on the nature of the cation balancing the negative charge of the zeolite framework (H^+ , Na^+ versus K^+), and is related to the size and the location of the cation. Larger K^+ ion coordinates preferably in sites on the channel intersection. The Na^+ cations occupy these sites as well as the sites on top of the six-membered ring on the channel wall [11].

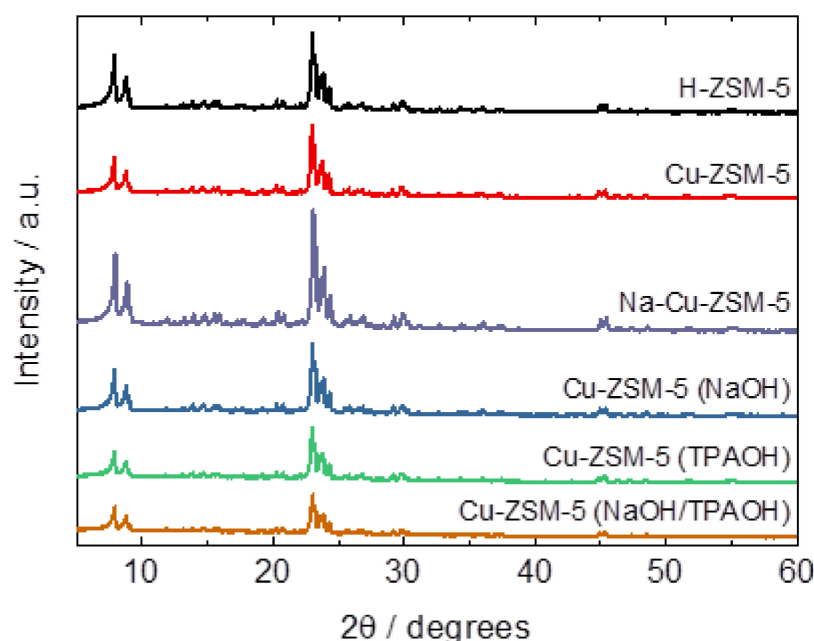


Figure 1. XRD patterns of H-ZSM-5, micro-/mesoporous Cu-exchanged ZSM-5 and Cu-exchanged ZSM-5 with co-cation (sample labels as in Table 1).

Table 1. Chemical analysis results determined from ICP-OES measurements and changes in the samples crystallinity determined by XRD.

Samples	Si/wt %	Al/wt %	Cu/wt %	Co-Cation/wt %	$n(\text{Si})/n(\text{Al})$	Cu Exchange Level/%	Cryst. Level/%
H-ZSM-5	38.9	2.9	-	-	12.3	-	100
Cu-ZSM-5	38.6	2.9	2.8	-	12.8	82	75
Na-Cu-ZSM-5	-	-	4.2	0.05 (Na)	-	-	131
Cu-ZSM-5 (NaOH)	36.0	3.1	2.7	-	11.2	74	83
Cu-ZSM-5 (TPAOH)	37.0	2.9	3.3	-	12.3	97	57
Cu-ZSM-5 (NaOH/TPAOH)	37.0	3.0	2.7	-	11.8	76	54

- not investigated.

Independently of the Cu-loading (2.7–3.3 wt %) and the porosity, any reflections typical of CuO (characteristic diffraction peak at 36.4°) and/or Cu_2O (characteristic diffraction peaks at 35.6° and 38.8°) were not recognized in diffractograms of Cu-containing materials. The lack of these reflections indicates presence of copper oxide species' in a very well dispersed form (possible crystallites of CuO_x are smaller than XRD detection level) or have amorphous nature. Modification of Na-ZSM-5 with copper ions also did not affect XRD patterns, as no reflections characteristic for alkali nor copper species were detected (Figure 1).

The chemical analysis as determined by inductively coupled plasma optical emission spectrometry (ICP-OES) (Table 1) revealed $n(\text{Si})/n(\text{Al})$ of 12.3 for H-ZSM-5, so slightly different from the intended value of 13.5 (given by the manufacturer). The applied post-synthetic modification procedure (concentration of an alkaline solution of 0.2 M with the duration time of 2 h) only slightly influenced the $n(\text{Si})/n(\text{Al})$ ratio of the micro-/mesoporous materials, i.e., Cu-ZSM-5 (NaOH) and Cu-ZSM-5 (NaOH/TPAOH), and did not influence the $n(\text{Si})/n(\text{Al})$ ratio of Cu-ZSM-5 (TPAOH). The use of TPAOH directly produced the protonic form of the zeolite upon calcination. The final ion exchange with NH_4NO_3 was

required, however, in the case of NaOH or NaOH/TPAOH treatment. Furthermore, the ion-exchange with copper cations did not affect the Al amount as the $n(\text{Si})/n(\text{Al})$ molar ratio of 11.2–12.3 is kept at the level found for native H-ZSM-5. While as can be seen from Figure 1 and Table 1, the crystallinity intensity of Cu-ZSM-5 (TPAOH; NaOH/TPAOH) was significantly decreased compared to parent ZSM-5, thus it can be concluded that the post-synthetic modification led to the extraction not only Si but also Al from the zeolite framework. As the $n(\text{Si})/n(\text{Al})$ molar ratio is preserved at the level of native H-ZSM-5, some fraction of Al bears the form of extra framework species (see Table 2 reporting the highest number of Lewis sites determined from pyridine adsorption).

Table 2. Acidic properties of the samples determined from pyridine adsorption: concentration of Brønsted and Lewis sites, respectively ($C_{\text{Brønsted}}$, C_{Lewis}), total concentration (C_{Total}).

Samples	$C_{\text{Brønsted}}/\mu\text{mol g}^{-1}$	$C_{\text{Lewis}}/\mu\text{mol g}^{-1}$	$C_{\text{Total}}/\mu\text{mol g}^{-1}$
H-ZSM-5	635	0	635
Cu-ZSM-5	200	600	800
Na-Cu-ZSM-5	262	1280	1542
Cu-ZSM-5 (NaOH)	185	425	600
Cu-ZSM-5 (TPAOH)	60	1050	1100
Cu-ZSM-5 (NaOH/TPAOH)	255	735	990

The 2.8–3.3 wt % of the copper amount was able to be introduced to micro-/mesopores zeolites. The post-modification of H-ZSM-5 with TPAOH allowed the introduction of a higher amount of Cu species (3.3 wt %) compared to materials treated (before ion-exchange) with NaOH or NaOH/TPAOH. The tetraalkylammonium cations are not strongly solvated in an aqueous solution due to their effective cationic diameter, i.e., TPA^+ ca. 0.9 nm [12], and the hydrophobicity of their alkyl groups that interact with the hydrophobic silicate species rather than with polar water molecules [13,14]. In our case, the hydrophobic character of the zeolite could result in the deposition of a higher amount of copper species in aggregated forms, as can be seen in Figure 2. TEM imaging shows the presence of nanoparticles having size of 5–10 nm in all samples. Whereas in sample Cu-ZSM-5 and Na-Cu-ZSM-5 a homogeneous distribution of Cu nanoparticles is observed, the formation of agglomerates is assumed for the TPAOH treated sample (Figure 2c). These agglomerates could not be observed in all ZSM-5 particles of this sample (Figure 2d), but in all positions, the nanoparticle distribution looks more inhomogeneous compared to the untreated samples. Furthermore, in some ZSM-5 particles the arrangement of the agglomerates seems to be located in defects of the ZSM-5 crystals or on the external surface of zeolite grains. Furthermore, the ion-exchange with Cu ions in Na-ZSM-5 resulted in much higher accommodation of copper species (Cu wt %, Table 1) compared to microporous or micro-/mesoporous Cu-exchanged H-ZSM-5. A similar effect was observed for other co-cation (Na, K or Li)- and Cu-containing zeolites, e.g., Cu(Na,K,Li)-SSZ-13 [6] or Cu(Na)-Y [15], etc. One of the possible explanation for the difference between copper content in H-ZSM-5 and Na-ZSM-5 is that the pH of the copper-exchanging solution changes at the beginning of the exchange or during the exchange. The solution becomes more basic in the presence of Na-ZSM-5 and the formation of $\text{Cu}[(\text{OH})]^+$ may be favored. Thermal decomposition of $\text{Cu}[(\text{OH})]^+$ at exchange position results in the formation of $[\text{Cu}-\text{O}-\text{Cu}]^{2+}$, interacting with two charge-balancing framework Al sites in ZSM-5 [16]. The $\text{Cu}[(\text{OH})]^+$ ions can also precipitate as $\text{Cu}(\text{OH})_2$ crystallites but only at pH higher than those prevalent during ion-exchange (above pH 6) [17]. In our case the pH did not exceed a value of 5.70 ± 0.20 , thus, the formation of $\text{Cu}(\text{OH})_2$ after exchange and thermal treatment is unlikely with our preparation procedure.

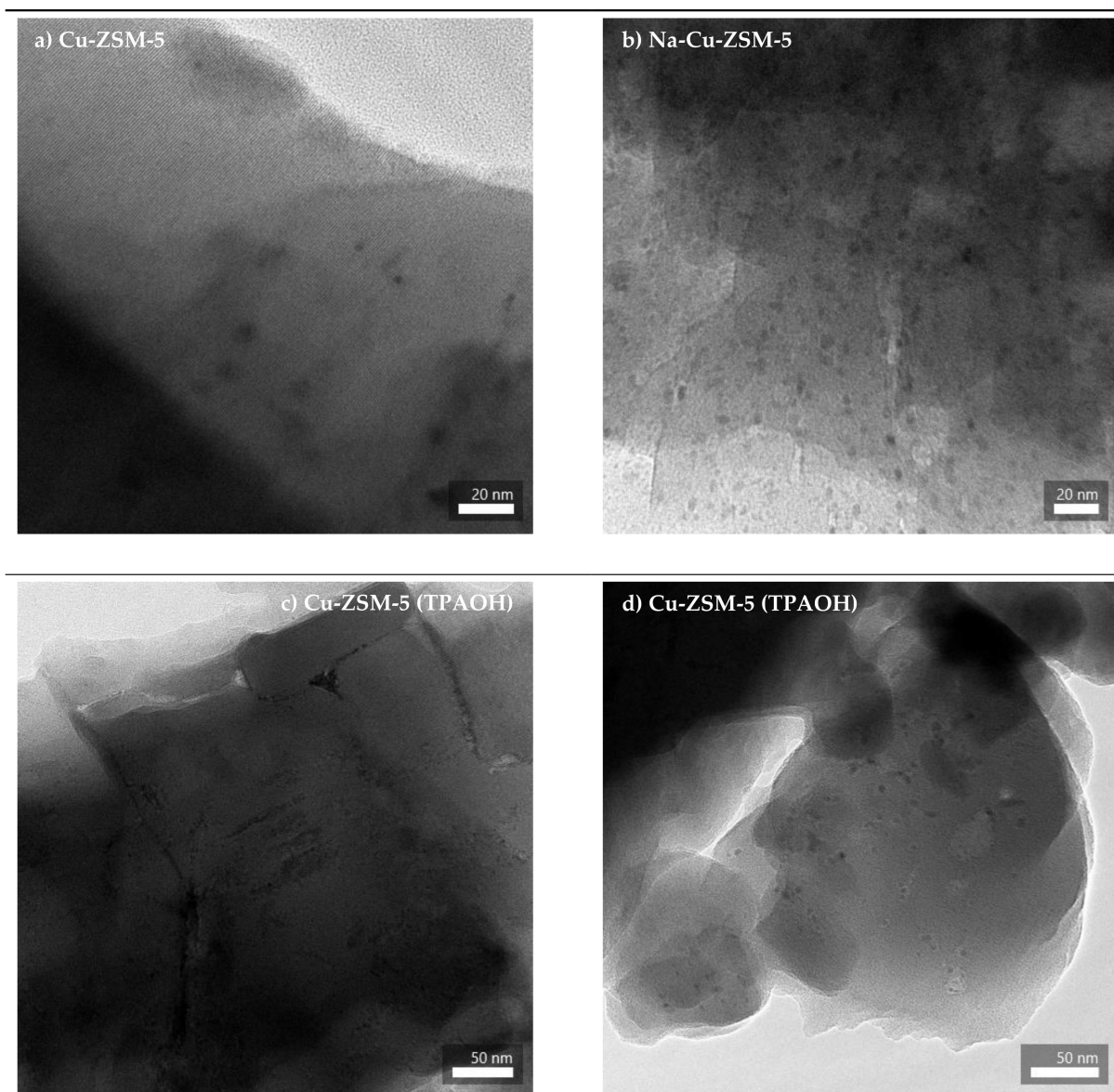


Figure 2. TEM images of selected Cu-exchanged ZSM-5, (a) Cu-ZSM-5, (b) Na-Cu-ZSM-5, (c,d) Cu-ZSM-5 (TPAOH).

Figure 3 presents the N_2 adsorption-desorption isotherms recorded for the selected Cu-exchanged ZSM-5 samples, while Table 3 presents the textural properties of the materials. The adsorption-desorption isotherm of H-ZSM-5 is of type IV(a), according to the IUPAC classification [18]. For the materials obtained after the post-modification with NaOH or NaOH/TPAOH and subsequent ion-exchange with copper ions, the shape of the isotherms is also of type IV(a) [18]. However, the Cu-ZSM-5 (NaOH) and Cu-ZSM-5 (NaOH/TPAOH) samples revealed a higher distribution of mesopores, i.e., the isotherm shows an increase of the adsorbed volume at a higher relative pressure (Figure 3a). The Na-Cu-ZSM-5 material revealed textural properties similar to Cu-ZSM-5. The post-modification with NaOH or NaOH/TPAOH and subsequent ion-exchange with copper increased the values of specific surface area and volume of mesopores as compared to H-ZSM-5 and Cu-ZSM-5. Although by using NaOH, most of the mesoporosity was reported to develop in the first 15 min of the treatment [19,20], we applied the condition (i.e., the concentration of 0.2 M, the time duration of 2 h, the temperature of treatment of 65 °C) to the one reported before for the materials dedicated to NH_3 -SCR [3,21].

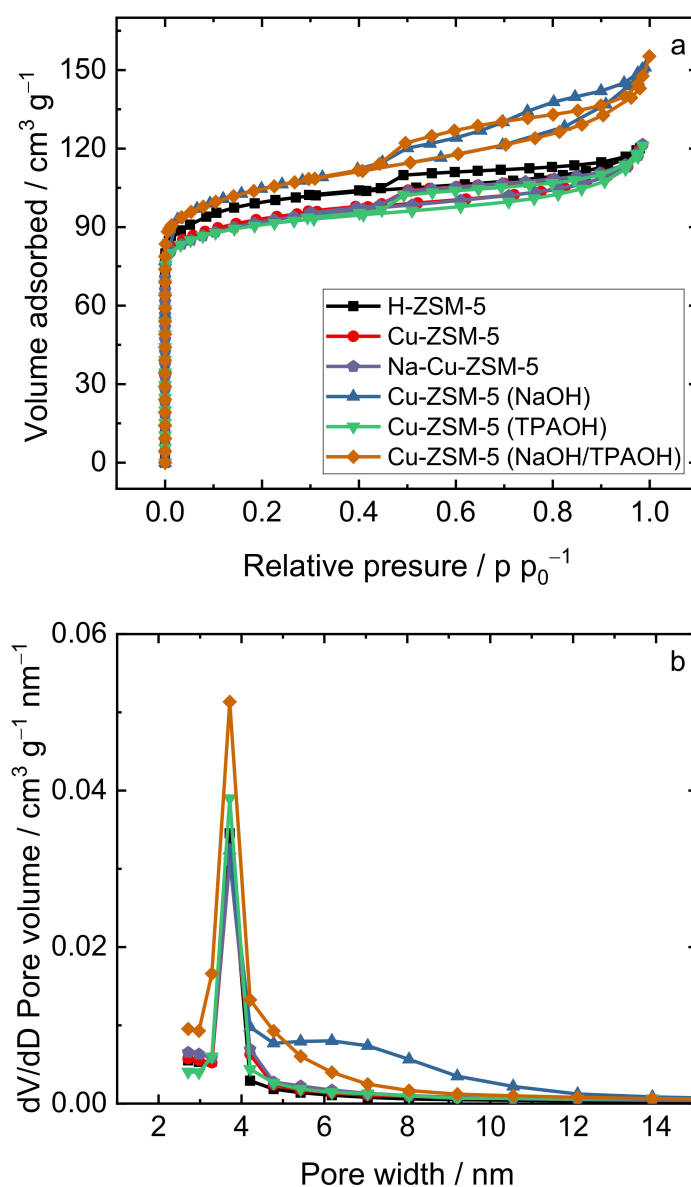


Figure 3. (a) N₂-adsorption isotherms and (b) pore size distribution of H-ZSM-5, micro-/mesoporous Cu-exchanged ZSM-5 and Cu-exchanged ZSM-5 with co-cation.

Table 3. Textural properties of the samples determined from the N₂-adsorption measurements: specific surface area (a_s(BET)), micropore pore volume (V_{MIC}), mesopore pore volume (V_{MES}) and total pore volume (V_{TOT}).

Samples	a _s (BET)/m ² g ⁻¹	V _{MIC} /cm ³ g ⁻¹	V _{MES} /cm ³ g ⁻¹	V _{TOT} /cm ³ g ⁻¹
H-ZSM-5	318	0.14	0.05	0.19
Cu-ZSM-5	296	0.13	0.06	0.19
Na-Cu-ZSM-5	296	0.12	0.07	0.19
Cu-ZSM-5 (NaOH)	329	0.13	0.10	0.23
Cu-ZSM-5 (TPAOH)	290	0.13	0.06	0.19
Cu-ZSM-5 (NaOH/TPAOH)	337	0.13	0.10	0.23

The post-modification with TPAOH did not lead to mesoporosity formation. Albelló et al. [22] reported minor alteration of the porosity and chemical composition of H-ZSM-5 ($n(\text{Si})/n(\text{Al}) = 42$) in 1 M TPAOH at 65 °C for 30 min. The authors explained the results based on the limited attack by OH⁻ to Si-OH defects and thus increasing the roughness of the crystal's external surface. In our case, the significantly lower concentration of TPAOH (0.2 M) resulted in the preserved textural properties with respect to the parent sample. It should be stressed that only one reference TPAOH treatment (0.2 M, 2 h, 65 °C) was considered in this work for comparison with NaOH treatment. Otherwise, the structure of the applied H-ZSM-5 was not preserved after the application of other conditions, i.e., concentration of TPAOH of 1 M, 2–8 h, 65 °C. The investigations in the post-synthetic treatment (different concentrations, time, temperature, etc.) of ZSM-5 in TPAOH should be performed in separate studies.

Table 2 gathers the acidic properties of the samples as determined by pyridine (Py) adsorption. The H-ZSM-5 zeolite accommodates Brønsted acid sites only. After the introduction of copper ions to native and post-modified supports the 3–3.5 fold decrease in the concentration of Brønsted acid sites is observed what is accompanied by the appearance of Lewis acid sites. While for the non-modified supports the Lewis acid sites originate from Cu cationic species, in post-modified materials in addition to Cu-Lewis sites the coexistence of Al-species should be considered. For the Cu-ZSM-5 (TPAOH) catalyst, the lowest concentration of Brønsted acid sites is also determined which suggests the presence of Cu⁺ and/or Cu²⁺ cations balancing the negative charge of zeolite framework instead of protons, so for high dispersion of copper sites. The highest concentration of Lewis sites also confirms the observations mentioned above for Cu-ZSM-5 (TPAOH). It is in line with the highest amount of copper (3.3 wt %, based on ICP-OES analysis versus 2.7 wt % for Cu-ZSM-5 (NaOH) and Cu-ZSM-5 (NaOH/TPAOH)). This high accessibility of Lewis sites to Py molecules also indicates that the aggregated particles of Cu species formed selectively in Cu-ZSM-5 (TPAOH) (the TEM analysis (Figure 2)) are located on the external surface of zeolite grains.

Furthermore, it is important to note that the co-cations (Na⁺) cannot fully replace all Brønsted acid sites (H⁺). Gao et al. [6] correlated an efficiency for co-cations in exchanging H⁺ (increasing as follows: Li⁺ < Na⁺ < K⁺) to their effective diameters in a hydrated form. Further, the source of Brønsted acidity in Na-Cu-ZSM-5 is the hydrolysis of Cu²⁺ aqua complexes, i.e., [Cu(OH)]⁺ that provides both Cu-oxo species and H⁺ cations. Indeed, the share of Cu²⁺_{exch+oxo} sites is the highest for Na-Cu-ZSM-5 as can be derived from quantitative IR studies of CO adsorption. The inspection into the spectra of Py interacting with surface acidic sites provides information not only on the sites' density. The position of PyL band contains information on both the heterogeneity and the strength of Lewis sites: the higher PyL band position is the higher strength the Lewis sites possess. Two types of Lewis acid sites, related to copper sites of different electron acceptor properties, are populated in the studied samples (Figure 4), as identified by 1454 and 1450 cm⁻¹ PyL bands. Most electron-acceptor sites are accommodated in Cu-ZSM-5 and both alkali treatment and modification with Na⁺ ions result in their strength lowering. Judging from the variety of copper forms that can serve as Lewis acid sites it is impossible to determine the concentration of Na⁺ and Cu⁺ independently from each other.

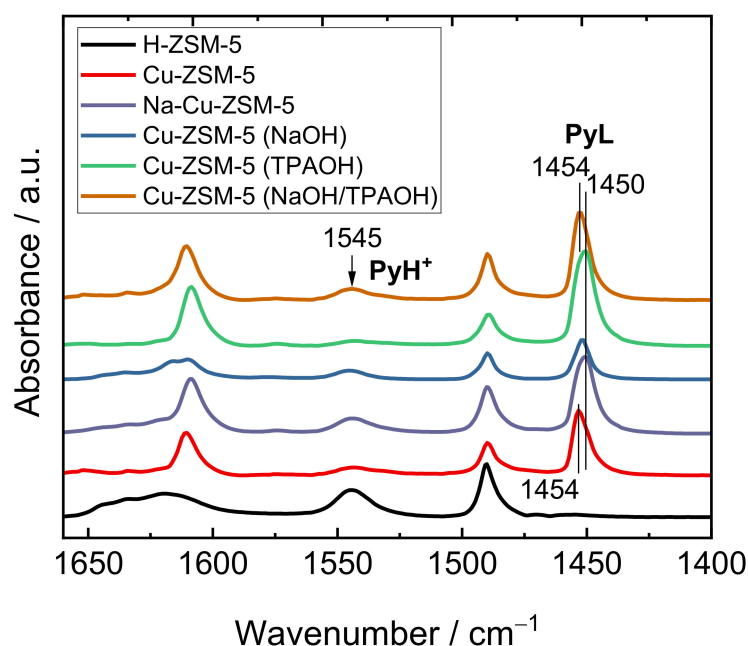


Figure 4. FT-IR spectra of adsorbed pyridine on H-ZSM-5, micro-/mesoporous Cu-exchanged ZSM-5 and Cu-exchanged ZSM-5 with co-cation.

2.2. Status of Copper Species

Figure 5 shows the ultraviolet-visible diffuse reflectance spectra (DR UV-Vis) of the studied samples (calcined at 500 °C, 4 h, air). The adsorption bands at about 210 and 251 nm are present over pure H-ZSM-5, and these bands can be assigned to the zeolite structure (band-originating from the charge transfer O_2-Al^{3+} and surface defects, respectively) [3,23]. For all Cu-containing materials two distinct bands in DR UV-Vis spectra appeared. The charge transfer band at around 211–214 nm is related to $O \rightarrow Cu$ charge transition (CT) from lattice oxygen to isolated Cu^+/Cu^{2+} species stabilized by the zeolite framework [24,25]. The broad absorption band between 550 and 900 nm is assigned to the d-d transitions of Cu^{2+} ions in pseudo-octahedral coordination (e.g., $Cu(H_2O)_6^{2+}$) [24,25]. Additional bands at around 255 nm (especially visible in the spectra recorded for Cu-ZSM-5 (TPAOH)) and 325 nm, were attributed to CuO species and the oligomeric $[Cu-O-Cu]^{2+}$ chains [26]. Cu-ZSM-5 (TPAOH) possesses higher amount of copper content (3.3 wt %) compared to the other materials, i.e., Cu-ZSM-5 (NaOH) and Cu-ZSM-5 (NaOH/TPAOH) with the copper content of 2.7 wt %. The DR UV-Vis data also support the FT-IR results that allow us to conclude on the presence of a high concentration of isolated Cu^+ and Cu^{2+} ions and a high content of oxide species in Cu-ZSM-5 (TPAOH). The DR UV-Vis spectrum for material modified with Na^+ as co-cation and further with copper ions don't show any new bands (as indicated above). Interestingly, Na-Cu-ZSM-5 revealed a higher content of copper (4.2 wt %, based on ICP-OES analysis, Table 1) compared to Cu-ZSM-5 (TPAOH), thus a higher contribution of aggregated copper species can be expected. The small half-width of 214 nm band in Na-Cu-ZSM-5 suggests the homogeneity of Cu^+/Cu^{2+} species engaged into interaction with zeolite framework. Further, its lower intensity among all materials tested indicates that Na^+ ions replaced copper cations in exchange positions forcing the copper to form oxo-species. As can be seen from the spectrum for this material (300–600 nm), the presence of co-cation promoted the evolution of $[Cu-O-Cu]^{2+}$ dimers (ca. 325 nm). Further temperature-programmed measurements (TPD- NO_x) were carried out to prove promoted the development of copper-oxo-species.

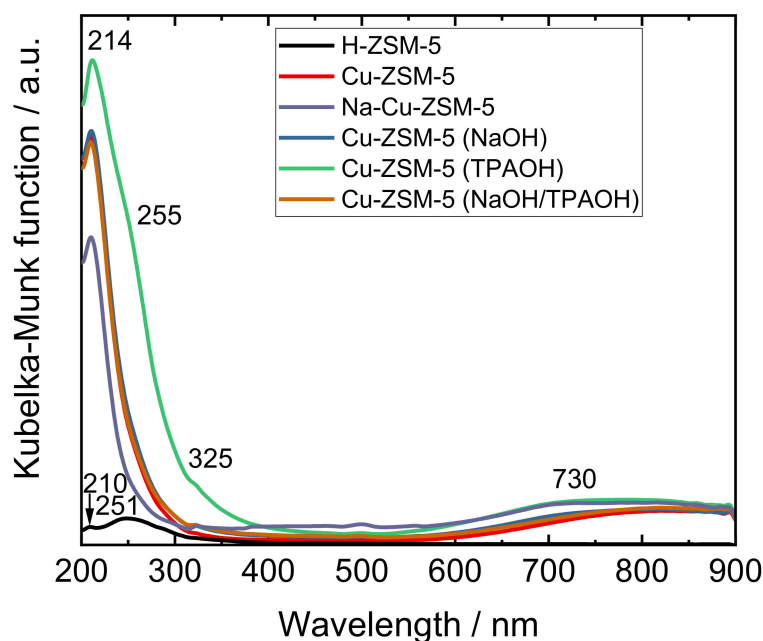


Figure 5. DR UV-Vis spectra of H-ZSM-5, micro-/mesoporous Cu-exchanged ZSM-5 and Cu-exchanged ZSM-5 with co-cation.

Figure 6 shows the experimental (solid line) and modeled (dashed line) TPD- NO_x profiles obtained for H-ZSM-5 as well as Cu-exchanged ZSM-5 via desorption (Supplementary Materials Figure S1) in the flow of (4 vol.%) O_2/He mixture. Table 4 gathers the results of the amounts of NO and NO_x adsorbed on the studied materials while Supplementary Materials Table S1 presents the kinetic parameters that are relevant to adsorption and desorption studies. The catalysts stored substantially more NO_x compared to NO. For H-ZSM-5, the peak at ca. 250 °C is likely associated with NO^+ interacting with the anionic zeolite site, forming $\text{Z}-\text{NO}^+$: $2\text{Zeo}-\text{O}^- - \text{H}^+ + \text{NO}_2 + \text{NO} \leftrightarrow 2\text{Zeo}-\text{O}^- - \text{NO}^+ + \text{H}_2\text{O}$ [27]. The activation energy of desorption of only 37 kJ mol^{-1} was the lowest among all the materials, which results in a low-temperature influence on the desorption rate: broad and weak intensity desorption peak is observed during the heat-up. The Cu-ZSM-5 (TPAOH) sample shows higher adsorption capacity than other materials, i.e., Cu-ZSM-5 (NaOH) and Cu-ZSM-5 (NaOH/TPAOH). Additionally, the two NO_x peaks in the profile of such materials indicate that NO_x binds to at least two different sites with distinct binding energies. Again, this effect can be assigned to the higher concentration of copper present in Cu-ZSM-5 (TPAOH), and thus, aggregated copper species. The desorption peak below 150 °C corresponds to the NO molecules that desorb from the isolated $\text{Cu}^+/\text{Cu}^{2+}$ [28,29]. The peak between 340–360 °C is assigned to the desorption of NO_2 formed in the reaction between NO and the $[\text{Cu}-\text{O}-\text{Cu}]^{2+}$ active sites [28]: $\text{NO} + [\text{Cu}-\text{O}-\text{Cu}]^{2+} \rightarrow \text{NO}_2 + [\text{Cu}-\square-\text{Cu}]^{2+}$. The activation energy of desorption is very high (84 kJ mol^{-1} for Cu-ZSM-5), demonstrating strong interaction between NO and $[\text{Cu}-\text{O}-\text{Cu}]^{2+}$ sites. The peak at ca. 250 °C originates from the thermal decomposition of nitrate and/or nitrite species generated by NO adsorption on $[\text{Cu}-\text{O}-\text{Cu}]^{2+}$ [30,31]: $2\text{NO} + [\text{Cu}-\text{O}-\text{Cu}]^{2+} \rightarrow \text{Cu}^+ - \text{NO} + [\text{Cu}-\text{NO}_2]^+$. This energy barrier is lower (42–45 kJ mol^{-1}) and the desorption rate is the highest at lower temperatures for Cu-ZSM-5 (NaOH/TPAOH) and Cu-ZSM-5 (NaOH), i.e., the materials with introduced mesoporosity. A significant increase in adsorption capacity for NO_x is observed for material containing co-cation (Na^+) and Cu ions, which is in agreement with previous studies, showing that Na^+ in the zeolite-based catalysts are favorable for NO_x storage [e.g., [31,32]].

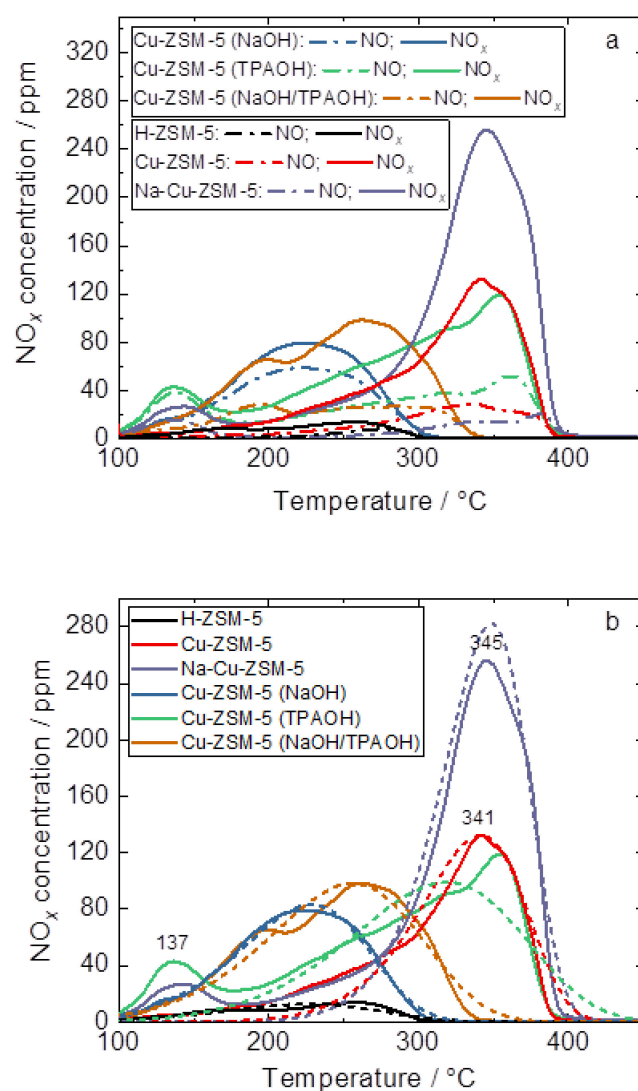


Figure 6. (a) TPD- NO_x (desorption of NO and NO_x) profiles and (b) TPD- NO_x (desorption of NO_x) profiles (solid measured, dashed modeled) of H-ZSM-5 and micro-/mesoporous Cu-exchanged ZSM-5 and Cu-exchanged ZSM-5 with co-cation, carried out in the flow of (4 vol.%) O_2/He mixture.

Table 4. NO_x adsorption capacity of H-ZSM-5 and Cu-exchanged ZSM-5 carried out in the flow of (4 vol.%) O_2/He mixture (data corresponding to results shown on Figure 6).

Sample	$C_{\text{NO}}/\mu\text{mol g}^{-1}$	$C_{\text{NO}_x}/\mu\text{mol g}^{-1}$
H-ZSM-5	4	10
Cu-ZSM-5	19	68
Na-Cu-ZSM-5	13	121
Cu-ZSM-5 (NaOH)	39	50
Cu-ZSM-5 (TPAOH)	46	89
Cu-ZSM-5 (NaOH/TPAOH)	26	69

Furthermore, the effect of a mixture of NO/He, NO/ O_2 /He and NO/ O_2 /H $_2$ O/He on the adsorption of NO was studied by carrying out NO adsorption and TPD tests on Cu-ZSM-5, Cu-ZSM-5 (TPAOH) and Na-Cu-ZSM-5 to quantitatively determine the species affected by O_2 and H $_2$ O up to 450 °C (Figure 7). The oxidation of NO to NO_2 did not appear on the lattice oxygen of Cu-exchanged ZSM-5, pronounced by the same adsorption capacity. The presence of O_2 in the feed mixture enhanced NO adsorption, especially in the case of Cu-ZSM-5(TPAOH) and Na-Cu-ZSM-5, thus the materials containing aggregated

copper oxides. Additionally, the presence of H₂O strongly reduced NO adsorption by its displacement from copper sites, as reported by Landi et al. [33]. However, the reduction of NO_x adsorption by water could not be the main factor influencing the catalytic results (see Section 2.3. Catalytic and Spectroscopic Investigations—NH₃-SCR).

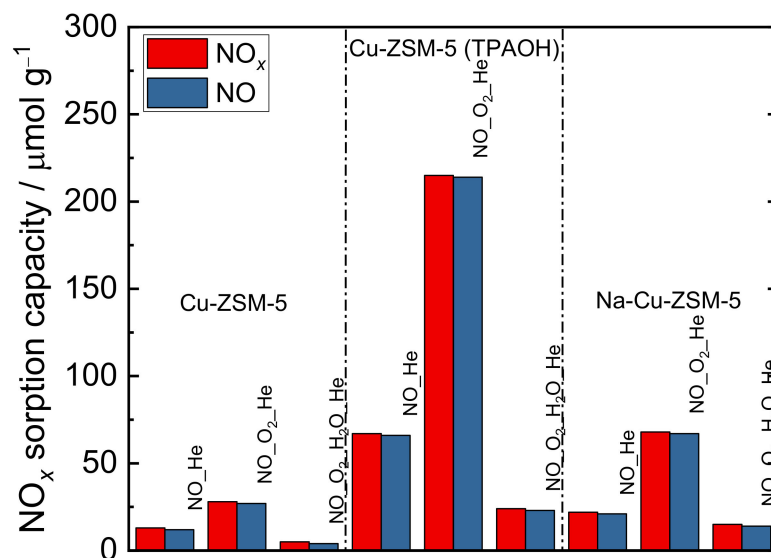


Figure 7. NO_x adsorption capacity of the selected Cu-exchanged ZSM-5.

Figure 8a shows the EPR spectra of hydrated (calcined at 550 °C, 4 h, air) Cu-exchanged ZSM-5 samples acquired at −196 °C (see Figure S2 for room temperature spectra) to characterize monomeric copper species. Closely related Cu²⁺ ions, such as [Cu–O–Cu]²⁺ and CuO species, are EPR silent due to the strong dipolar coupling [34,35]. Moreover, Cu⁺ is also silent because of its diamagnetic nature. In the region of the main Δm_s = 1 transitions, the typical copper hyperfine structure is well resolved, in agreement with previous studies [36,37]. Considering an axial symmetry for Cu centers, the well-defined low-field features correspond to the parallel component of the EPR signal, whereas the perpendicular part is characterless because of broadening arising from small unresolved couplings and inhomogeneous contributions of the sites. A single Cu monomer can be identified from the spectra of the three different zeolite samples and it has been attributed to octahedrally coordinated hydrated copper ions in Cu-exchanged ZSM-5 [38]. This species is free to move at room temperature and it has been located at the intersection of the zeolite channels. The relative intensities of the samples were calculated as the double integral of the signal at −196 °C and normalized concerning the weight of each measured sample. Na-Cu-ZSM-5 has the highest intensity and, thus, the highest Cu²⁺ concentration. Therefore, Cu-ZSM-5 (TPAOH) and Cu-ZSM-5 intensities, relatively to Na-Cu-ZSM-5 one, changed from 0.83 to 0.14, respectively.

The dehydration treatment led to a narrowing of the EPR line in agreement with the change of the Cu ions' coordination sphere with respect to the hydrated case. Moreover, the total intensity of the EPR spectra decreased by 60–70% when comparing to the fresh form of the samples, in agreement with previous investigations over copper-exchanged zeolites [39,40]. The appearance of two kinds of monomeric copper species upon water removal can be easily deduced from the low field region of the spectra in Figures 8b and 9 and can be assigned to the presence of two different extra-framework copper sites for copper interacting with the zeolitic oxygens. The fitted spin Hamiltonian parameters used for the simulation of the spectra are reported in Table 5. One group (named as A) has the typical parameters of a four-coordinated Cu²⁺ ion in a distorted square planar environment whereas the other one (labeled B) has a square pyramidal-5-coordinated geometry due to its higher g_{||} value and lower A_{||} component concerning A. The parameters found are in agreement with all the previous experimental and theoretical studies (e.g., [37,41]).

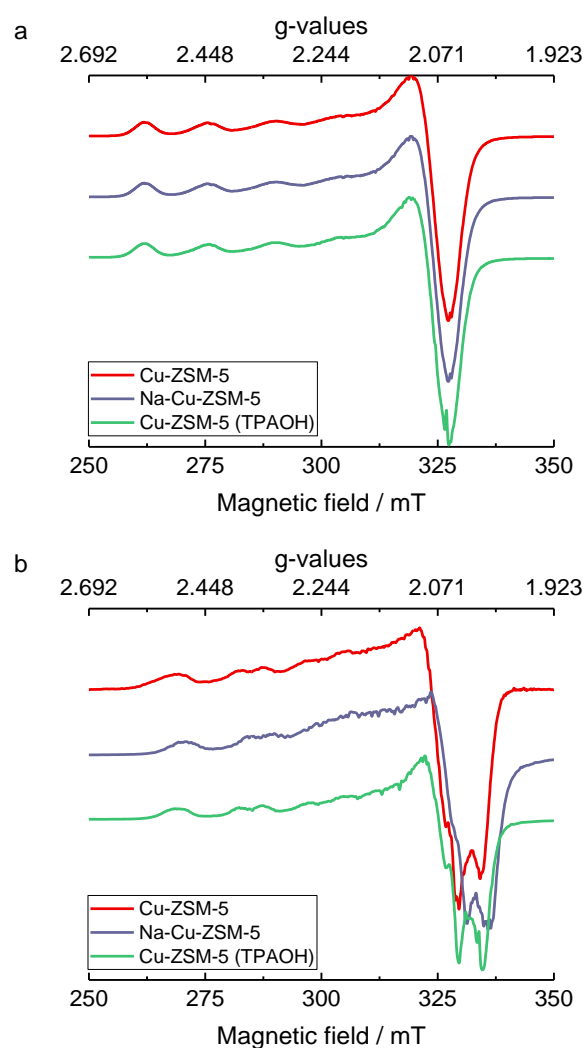


Figure 8. EPR spectra of: (a) hydrated (calcined at 500 °C, 4 h, air) and (b) dehydrated Cu-exchanged ZSM-5 recorded at -196 °C. The complete dehydration was achieved at 200 °C for 1 h in dynamic vacuum reaching a final pressure of 10^{-3} mbar.

The assignment of the experimental EPR signals to a specific exchange-site in ZSM-5 structure has been extensively investigated (e.g., [36,42]). Considering the MFI framework, ZSM-5 zeolites have four kinds of rings in their structure suitable for hosting copper ions: the sites located in six-membered rings are known as α , β , γ whereas the ones in five-membered rings are called δ [36]. According to Groothaert et al. [43], Cu(II) ions belonging to A come up at higher copper content ($n(\text{Cu})/n(\text{Al})$ of about 0.16 or higher). These are located, therefore, in less stable sites than the ones occupied by species of group B, already present at the lower copper concentration ($n(\text{Cu})/n(\text{Al})$ of about 0.007). They assigned species of group B to a three-, four- or five-coordinated Cu^{2+} ion in α rings with 1 or 2 aluminum atoms and species of group A to a four-coordinated Cu^{2+} located in all the other rings. Nevertheless, EPR signals' attribution to specific sites in dehydrated ZSM-5 materials is challenging because of its complicated structure. In our samples, the Cu concentration is high enough to have both A and B: the composition of groups A and B used in the simulations is 1:1 proving that the suitable exchange-sites are equally populated at high concentration of copper. As a result of this, the dehydrated samples show the presence of the same two Cu groups in the same amount. The minor discrepancies found in g_{\parallel} and A_{\parallel} values of a same group in the three samples confirms Groothaert's assignment pointing out that a variety of sites has to be considered for each group.

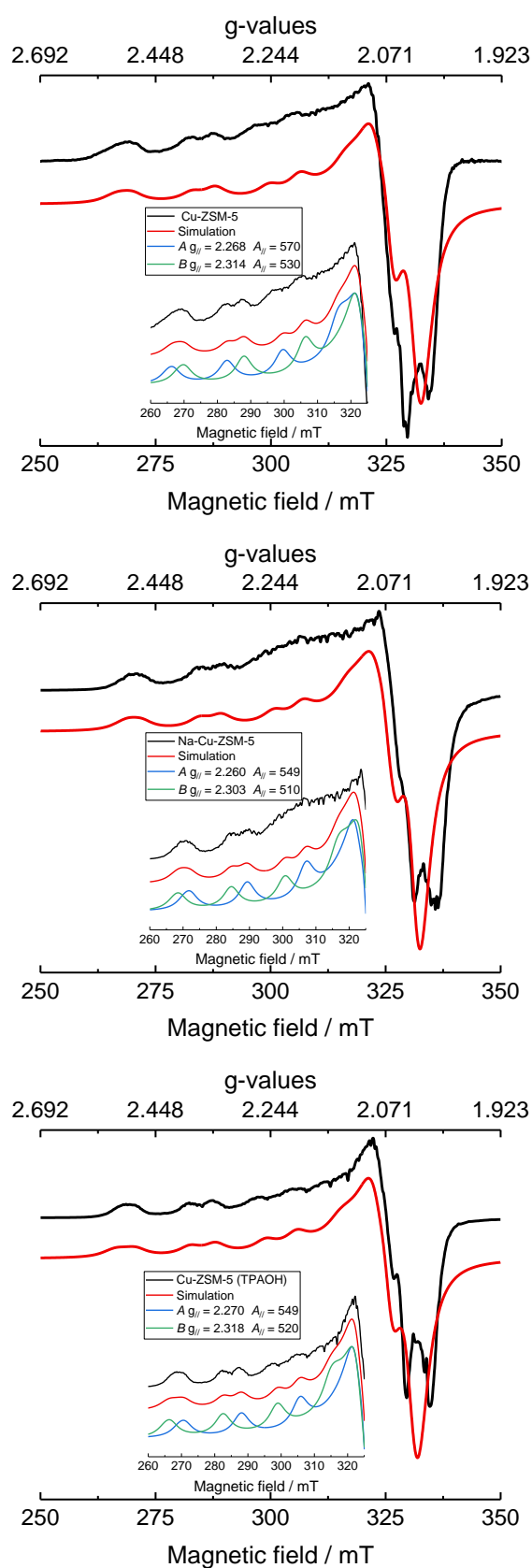


Figure 9. Experimental (black) and simulated (red) spectra of the dehydrated Cu-exchanged ZSM-5. The low field part of the experimental and simulated spectrum is reported on the bottom left of each spectrum. The simulation is obtained by summing the spectra of two different Cu species (A in blue and B in green) with a proper weight.

Table 5. Spin Hamiltonian parameters and broadening values (lwpp) used for the simulations of Cu species in the activated (dehydrated) Cu-exchanged ZSM-5.

Samples	Species	g_{\perp}	g_{\parallel}	A_{\perp} /MHz	A_{\parallel} /MHz	lwpp/mT
Cu-ZSM-5	A	2.073 ± 0.002	2.268 ± 0.001	40 ± 10	570 ± 5	$+3.3 \pm 0.5$
	B	2.068 ± 0.002	2.314 ± 0.001	40 ± 10	530 ± 4	$+3.3 \pm 0.5$
Na-Cu-ZSM-5	A	2.073 ± 0.002	2.260 ± 0.001	40 ± 10	549 ± 5	$+3.3 \pm 0.5$
	B	2.063 ± 0.002	2.303 ± 0.001	40 ± 10	510 ± 4	$+3.3 \pm 0.5$
Cu-ZSM-5 (TPAOH)	A	2.073 ± 0.002	2.270 ± 0.001	40 ± 10	549 ± 5	$+3.3 \pm 0.5$
	B	2.068 ± 0.002	2.318 ± 0.001	40 ± 10	520 ± 4	$+3.3 \pm 0.5$

To summarize, the main difference between the samples can be attributed to the quantity of monomeric Cu^{2+} ions detected in the hydrated state: the amount of EPR active Cu species in Cu-ZSM-5 sample (relative intensity 0.14) is seven times lower with respect to the Na-Cu-ZSM-5 sample (relative intensity 1.00) confirming the higher ion-exchange capabilities when co-cation is already accommodated.

In order to delve more clearly into the nature of copper centers, the studies of low-temperature CO adsorption were carried out. The CO molecule is very sensitive to copper oxidation state thus the position of the $\text{C}\equiv\text{O}$ bond vibration allows to conclude on both the presence of Cu^+ and Cu^{2+} cations and their agglomeration if they bear the form of the oxides. Figure 10a presents the spectra of CO adsorbed at room temperature (RT) on Cu-exchanged ZSM-5 as an example. At room temperature the interaction of CO with copper sites in zeolite results in the appearance of a strong band at 2157 cm^{-1} of $\text{Cu}^+(\text{CO})$ and a much weaker band at 2141 cm^{-1} of $\text{Cu}^{2+}_{\text{oxo}}(\text{CO})$. The $\text{Cu}^{2+}_{\text{oxo}}(\text{CO})$ and $\text{Cu}^{2+}_{\text{exch}}(\text{CO})$ monocarbonyls (denoted herein $\text{Cu}^{2+}_{\text{exch+oxo}}(\text{CO})$) are found at $2210\text{--}2200\text{ cm}^{-1}$ frequency range if the CO adsorption is performed at temperatures as low as $-100\text{ }^{\circ}\text{C}$ (Figure 10b). On the basis of the intensities of the monocarbonyl bands, i.e., ($\text{Cu}^+_{\text{exch}}(\text{CO})$), ($\text{Cu}^+_{\text{oxo}}(\text{CO})$), and $\text{Cu}^{2+}_{\text{exch+oxo}}(\text{CO})$ and the values of the absorption coefficient of the respective monocarbonyl bands [44] the concentrations of copper sites was calculated (Table 6). While the relative variations in the concentration of Cu^+ cations do not exceed 20% the variations in copper sites concentrations that are observed for $\text{Cu}^{2+}_{\text{exch+oxo}}$ and Cu^+_{oxo} species are significantly more important. Na-Cu-ZSM-5 and Cu-ZSM-5 (TPAOH) accommodate the highest number of oxo-species easily accessible for CO molecules (thus for NH_3 -SCR reactants due to similar kinetic diameter), further the amount of copper (II) oxo-species is the highest among all the studied materials. In Cu-ZSM-5, Cu-ZSM-5 (TPAOH/NaOH) and Cu-ZSM-5 (NaOH), the population of copper ions that in the exchange positions is similar to the Cu^+ and Cu^{2+} in oxide forms. Considering the Cu-exchanged ZSM-5 containing co-cation, it is visible that the presence of Na^+ results in the increased formation of Cu^+ . Additionally, Sultana et al. [4] elucidated the influence of Na^+ co-cation on the appearance of Cu^+ species in Cu-ZSM-5. They found that the concentration of Cu^+ species increased with an increase in the residual sodium content from 0.04 to 0.3 wt %. The variety of copper (II) monocarbonyls appeared due to the interaction of the probe with copper (II) sites of various electron-acceptor properties ($2220\text{--}2190\text{ cm}^{-1}$). The bands of the highest frequencies are found for the Na-Cu-ZSM-5 (2216 cm^{-1}) and Cu-ZSM-5 (TPAOH) (2205 cm^{-1}) materials what allows concluding on the highest electron-acceptor properties of copper (II) centers that they accommodate. The co-presence of Na^+ cations significantly affects the sites in Cu-ZSM-5; they are undoubtedly more electron-acceptor than in Cu-ZSM-5 (TPAOH) what finally can facilitated binding reagent molecules.

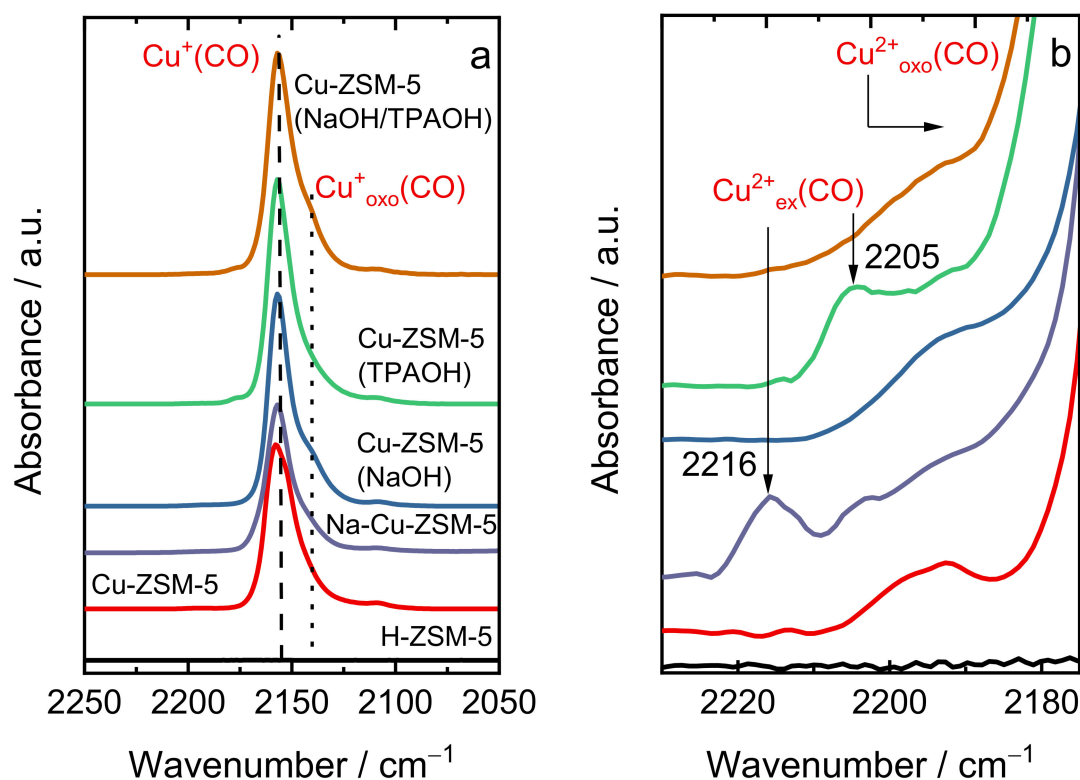


Figure 10. FT-IR transmission spectra of CO adsorbed at: (a) room temperature (RT) and (b) $-100\text{ }^{\circ}\text{C}$ in H-ZSM-5, micro-/mesoporous Cu-exchanged ZSM-5 and Cu-exchanged ZSM-5 with co-cation. The spectra present the maximum intensities of the copper (I) and copper (II) monocarbonyl bands.

Table 6. Concentration of copper sites derived from quantitative IR studies of CO adsorption: concentration of monocarbonyls ($C(\text{Cu}^+_{\text{exch}})$, $C(\text{Cu}^+_{\text{oxo}})$, $C(\text{Cu}^{2+}_{\text{exch+oxo}})$), and total concentration (C_{Total}).

Samples	$C(\text{Cu}^+_{\text{exch}})/\mu\text{mol g}^{-1}$	$C(\text{Cu}^+_{\text{oxo}})/\mu\text{mol g}^{-1}$	$C(\text{Cu}^{2+}_{\text{exch+oxo}})/\mu\text{mol g}^{-1}$	$C_{\text{Total}}/\mu\text{mol g}^{-1}$
Cu-ZSM-5	160	22	115	297
Na-Cu-ZSM-5	152	25	265	442
Cu-ZSM-5 (NaOH)	170	35	145	350
Cu-ZSM-5 (TPAOH)	185	15	295	495
Cu-ZSM-5 (NaOH/TPAOH)	190	30	120	340

2.3. Catalytic and Spectroscopic Investigations— NH_3 -SCR

Figure 11 shows the results of catalytic studies on H-ZSM-5 and Cu-ZSM-5 and the kinetic parameters of the relevant surface reactions are summarized in Table 7. Pure H-ZSM-5 shows gradual conversion only above $300\text{ }^{\circ}\text{C}$ (Figure 11a), while k_1^{surf} and TOF_1 for NH_3 -SCR at $150\text{ }^{\circ}\text{C}$, is five orders of magnitude lower than any other catalyst tested in this work. High NO conversions measured at the highest temperature indicates that the rate of the parallel parasitic ammonia oxidation reaction (r_2^{surf}) is negligible, therefore both relevant kinetic parameters have wide confidence intervals. However, it is clear that both k_2 and TOF_2 are below $2 \times 10^{-4}\text{ s}^{-1}$ and $2 \times 10^{-5}\text{ s}^{-1}$ respectively. On the other hand, the selectivity towards N_2O formation is by far the highest for H-ZSM-5. A significantly higher NO conversion was obtained for Cu-ZSM-5. Interestingly, there is no significant difference for the micro-/mesoporous materials, especially Cu-ZSM-5 (NaOH) and Cu-ZSM-5 (NaOH/TPAOH), both having the Ea_1^{surf} of around 105 kJ mol^{-1} . A slightly different conversion can be seen above $350\text{ }^{\circ}\text{C}$. In the presence of the Cu-ZSM-5 (TPAOH) catalyst, apparently a significantly higher loss in NO conversion above $350\text{ }^{\circ}\text{C}$ appears due

to the side reaction of NH_3 oxidation, having a much lower energy barrier $E_{a_2}^{surf}$ compared to other Cu-containing ZSM-5 catalysts. Additionally, for this material the highest N_2O formation rate was noticed (Figure 11b), confirmed by the corresponding surface rate constants. This behavior can be explained by the higher amount of copper in this material and thus, aggregated forms of copper species (i.e., $[\text{Cu-O-Cu}]^{2+}$ and CuO_x). Interestingly, the higher content of copper in Na-Cu-ZSM-5 (4.2 wt % of Cu, based on ICP-OES analysis), did not cause the oxidation of NH_3 above 350 °C, as was observed in the case of the Cu-ZSM-5 (TPAOH) sample. Otherwise, for Na-Cu-ZSM-5, a significantly higher amount (compared to the other samples) of desorbed NO_x in the presence of O_2/He mixture was observed (e.g., 68 and 121 $\mu\text{mol g}^{-1}$ for Cu-ZSM-5 and Na-Cu-ZSM-5, respectively). NO_x appears as a result of the reaction between NO and the $[\text{Cu-O-Cu}]^{2+}$ active sites (based on TPD- NO_x analysis). Thus, both Cu^{2+} and $[\text{Cu-O-Cu}]^{2+}$ species are considered as the active Cu species in NH_3 -SCR.

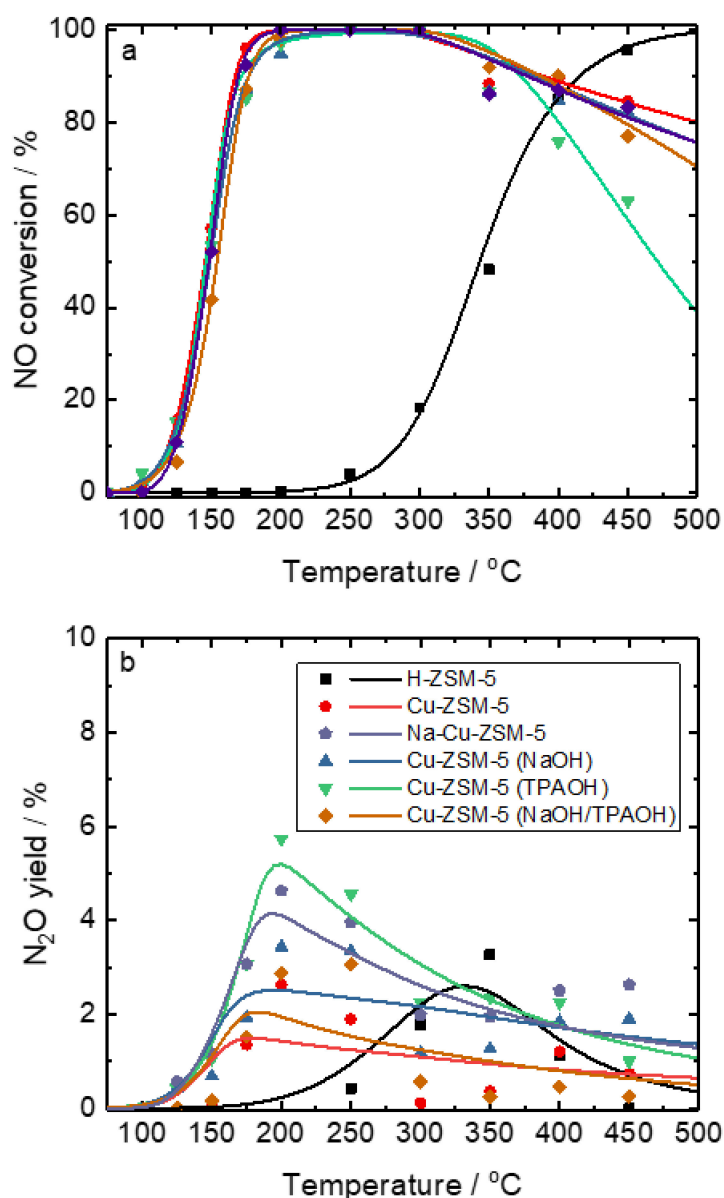


Figure 11. Experimental (points) and modeling (lines) results of catalytic studies: (a) NO conversion and (b) N_2O yield (reaction conditions: 0.2 g of catalyst, 120 mL min^{-1} , 500 ppm NO, 575 ppm NH_3 , 4 vol.% O_2 and He balance, GHSV = 30,000 h^{-1}).

Table 7. Calculated kinetic parameters for surface reactions.

	r_1^{surf}			r_2^{surf}			r_3^{surf}		
	AS-NH ₃ +AS-NO $\frac{1}{4}$ O ₂ →2AS+ $\frac{3}{2}$ H ₂ O+N ₂			AS-NH ₃ + $\frac{3}{4}$ O ₂ →AS+ $\frac{3}{2}$ H ₂ O + $\frac{1}{2}$ N ₂			AS-NH ₃ +AS-NO+ $\frac{3}{4}$ O ₂ →2AS+N ₂ O + $\frac{3}{2}$ H ₂ O		
	$k_1^{surf} \cdot \theta_{NO} \cdot \theta_{NH_3}$			$k_2^{surf} \cdot \theta_{NH_3}$			$k_3^{surf} \cdot \theta_{NO} \cdot \theta_{NH_3}$		
	* k_1^{surf}/s^{-1}	$Ea_1^{surf}/kJ mol^{-1}$	* TOF_1/s^{-1}	* k_2^{surf}/s^{-1}	$Ea_2^{surf}/kJ mol^{-1}$	* TOF_2/s^{-1}	* k_3^{surf}/s^{-1}	$Ea_3^{surf}/kJ mol^{-1}$	* TOF_3/s^{-1}
H-ZSM-5	$(3.9 \pm 0.4) \times 10^{-8}$	154 ± 1	3.06×10^{-9}	$(1 \pm 1) \times 10^{-4}$	58 ± 58	1.59×10^{-5}	$(1.0 \pm 0.3) \times 10^{-6}$	85 ± 4	7.99×10^{-8}
Cu-ZSM-5	$(1.7 \pm 0.1) \times 10^{-3}$	119 ± 3	1.50×10^{-4}	$(5.2 \pm 0.7) \times 10^{-3}$	143 ± 4	1.90×10^{-3}	$(3.2 \pm 0.9) \times 10^{-5}$	82 ± 5	2.73×10^{-6}
Na-Cu-ZSM-5	$(1.01 \pm 0.05) \times 10^{-3}$	156 ± 1	7.28×10^{-5}	$(3.8 \pm 0.4) \times 10^{-3}$	79 ± 1	1.20×10^{-3}	$(4.1 \pm 0.6) \times 10^{-5}$	152 ± 1	2.99×10^{-6}
Cu-ZSM-5 (NaOH)	$(2.4 \pm 0.2) \times 10^{-3}$	106 ± 2	1.89×10^{-4}	$(3.9 \pm 0.3) \times 10^{-3}$	87 ± 6	1.45×10^{-3}	$(7.1 \pm 1.9) \times 10^{-5}$	102 ± 5	5.51×10^{-6}
Cu-ZSM-5 (TPAOH)	$(6.0 \pm 0.4) \times 10^{-4}$	85 ± 2	1.01×10^{-4}	$(5.5 \pm 0.8) \times 10^{-3}$	101 ± 5	1.07×10^{-3}	$(3.0 \pm 0.9) \times 10^{-5}$	79 ± 3	5.07×10^{-6}
Cu-ZSM-5 (NaOH/TPAOH)	$(1.1 \pm 0.1) \times 10^{-3}$	104 ± 2	8.27×10^{-5}	$(2.7 \pm 0.6) \times 10^{-2}$	111 ± 20	8.41×10^{-4}	$(3.1 \pm 1.7) \times 10^{-5}$	93 ± 11	2.45×10^{-6}
** Cu-ZSM-5	$(2.19 \pm 0.05) \times 10^{-3}$	119 ± 3	1.86×10^{-4}	$(5.4 \pm 0.4) \times 10^{-4}$	143 ± 4	2.53×10^{-4}	$(1.2 \pm 0.6) \times 10^{-4}$	105 ± 1	1.05×10^{-5}
** Na-Cu-ZSM-5	$(1.09 \pm 0.07) \times 10^{-3}$	149 ± 3	7.75×10^{-5}	$(2.4 \pm 0.9) \times 10^{-4}$	131 ± 3	8.76×10^{-5}	$(4.6 \pm 1.3) \times 10^{-5}$	136 ± 2	3.26×10^{-6}
** Cu-ZSM-5 (TPAOH)	$(4.3 \pm 0.2) \times 10^{-4}$	94 ± 3	7.04×10^{-5}	$(3.1 \pm 0.7) \times 10^{-3}$	105 ± 10	3.93×10^{-4}	$(3.5 \pm 0.8) \times 10^{-5}$	82 ± 5	5.59×10^{-6}

* Reaction rate constants and (maximum) turnover frequencies (TOF) at steady state obtained for the surface reactions at 150 °C (400 °C for r2); ** in the presence of 5 vol.% H₂O.

The results show that ammonia oxidation occurs at temperatures above 350 °C, with and without water present in the feed, but the oxidation occurs to a lower degree if water was present (Figure 12). The kinetic parameters confirm this observation, apparent activation energy (Ea_2^{surf}) is higher when H₂O was present in the feed, while the TOF_2 dropped by the order of magnitude for all catalysts tested with and without water. The comparatively higher NO conversion occurs because ammonia oxidation is slower. The kinetic parameters confirm this statement, as kinetic parameters for the NH₃-SCR reaction remain nearly unaffected in the tests with water in the feed. The introduction of water may thus suppress the adsorption of NH₃ and facilitate higher NO conversion as discussed by Sjövall et al. [45] A slight increase of TOF_1 was indeed observed (Figure S3). The N₂O yield in the presence of water vapor varied among these selected samples. In the case of samples containing aggregated copper species, N₂O yield remains similar (in the whole studied temperature range, i.e., for Cu-ZSM-5 (TPAOH)) or even lower concentration (above 200 °C) in the presence of H₂O. For Cu-ZSM-5, the introduction of H₂O in the feed caused higher N₂O yield mostly below 250 °C, e.g., 14 ppm of N₂O was formed without H₂O at 200 °C and increased to 30 ppm in the presence of 5 vol.% of H₂O. The selected catalysts were therefore tested for 24 h at 350 °C in the presence of H₂O. As shown in Figure 13, the presence of water vapor did not affect the NH₃-SCR activity of Cu-exchanged ZSM-5, which revealed nearly complete NO removal from the reaction mixture up to 24 h.

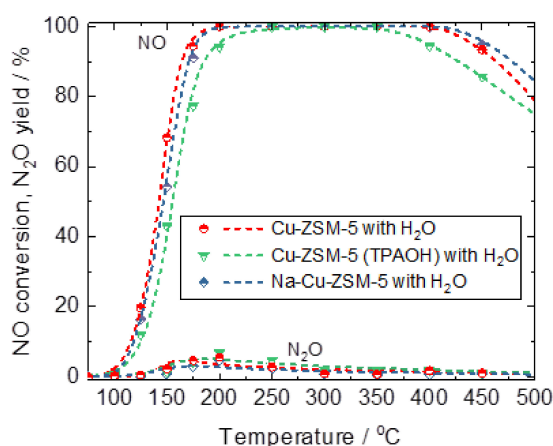


Figure 12. Results of catalytic studies: NO conversion and N₂O yield (reaction conditions: 0.2 g of catalyst, 120 mL min⁻¹, 500 ppm NO, 575 ppm NH₃, 4 vol.% O₂, 5 vol.% H₂O and He balance, GHSV = 30,000 h⁻¹).

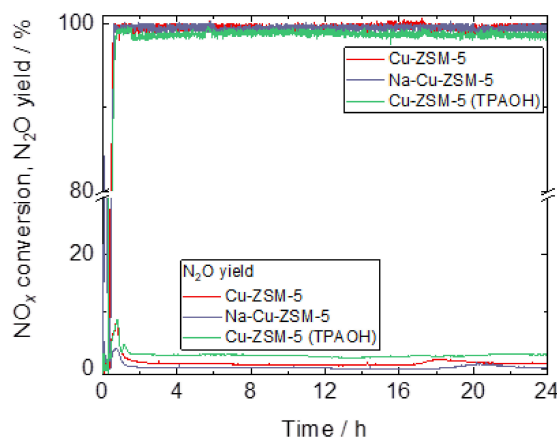


Figure 13. NO conversion and N₂O yield during NH₃-SCR over the Cu-exchanged ZSM-5 (reaction conditions: 0.2 g of catalyst, 120 mL min⁻¹, 500 ppm NO, 575 ppm NH₃, 4 Vol.% O₂, 5 Vol.% H₂O, and He balance, GHSV = 30,000 h⁻¹, 350 °C, 24 h).

The most important adsorption adducts and reaction intermediates can be easily identified in the FT-IR spectrum. The reagents (NO , O_2 and NH_3) in the stoichiometric amounts ($c(\text{NO})/c(\text{O}_2)/c(\text{NH}_3) = 4:1:4$) were contacted with the catalysts-Cu-ZSM-5, Na-Cu-ZSM-5 and Cu-ZSM-5 (TPAOH) at 150°C for 10 min then the FT-IR spectrum was collected (Figure 14). In the spectrum of reagents adsorbed on the studied materials the most intensive bands came from the species identified by the $1658\text{--}1640\text{ cm}^{-1}$ bands assigned to NO_3^- species. This indicates that NO can be easily oxidized to the surface nitrates upon contact with O_2 already at 150°C . The position of these bands strongly depends on the NO_3^- structure (speciation into monodentate, bidentate, or bridged entities), and on the kind of the cation to which they are bonded. The bands in the region of $1658\text{--}1640\text{ cm}^{-1}$ can also be considered as originating from ammonia molecules coordinatively bonded to Lewis acid sites, e.g., copper/sodium cations. The $1445\text{--}1430\text{ cm}^{-1}$ bands can originate from ammonium ions NH_4^+ appeared as the most characteristic moiety attributed to the reaction of ammonia with Brønsted sites (strongly acidic $\text{Si}(\text{OH})\text{Al}$ groups). On the other hand, the huge intensity of $1658\text{--}1640\text{ cm}^{-1}$ bands also justifies the attribution of the $1445\text{--}1430\text{ cm}^{-1}$ bands to monodentate nitrate species—the intermediate products of $\text{NH}_3\text{-SCR}$. The presence of NO_2^- is also manifested by the modes below 1400 cm^{-1} . The formation of NO_3^- is accompanied by the evolution of water (1615 cm^{-1}) because the nitrate anions replace surface OH groups. The water molecules are also the final reaction product of $\text{NH}_3\text{-SCR}$. The H_2O formation does not hinder the formation of nitrates. The significant intensities of nitrate species in Cu-ZSM-5 (TPAOH) signify that these intermediates are easily accumulated on the catalysts surface, their decomposition is not as effective as for Cu-ZSM-5 or even in Na-Cu-ZSM-5. The stability of nitrate species in Cu-ZSM-5 (TPAOH) and Na-Cu-ZSM-5 is supported by the formulation of N_2O in these materials in significant amounts. Therefore, the high concentration of Cu^{2+} oxo species (IR studies, Figure 10, Table 6) of low dispersion facilitates the production of N_2O by stabilizing nitrate intermediates on the catalyst surface. The presence of water in the feed (5 vol.%) inhibits the decomposition of $\text{NO}_3^-/\text{NO}_2^-$ and NH_4^+ species. Their amount on the catalysts surface is nearly 3-fold higher than in water-free conditions. The accumulation of the intermediate moieties is accompanied by the higher production of N_2O (Figure 15b). This effect is most pronounced for Cu-ZSM-5.

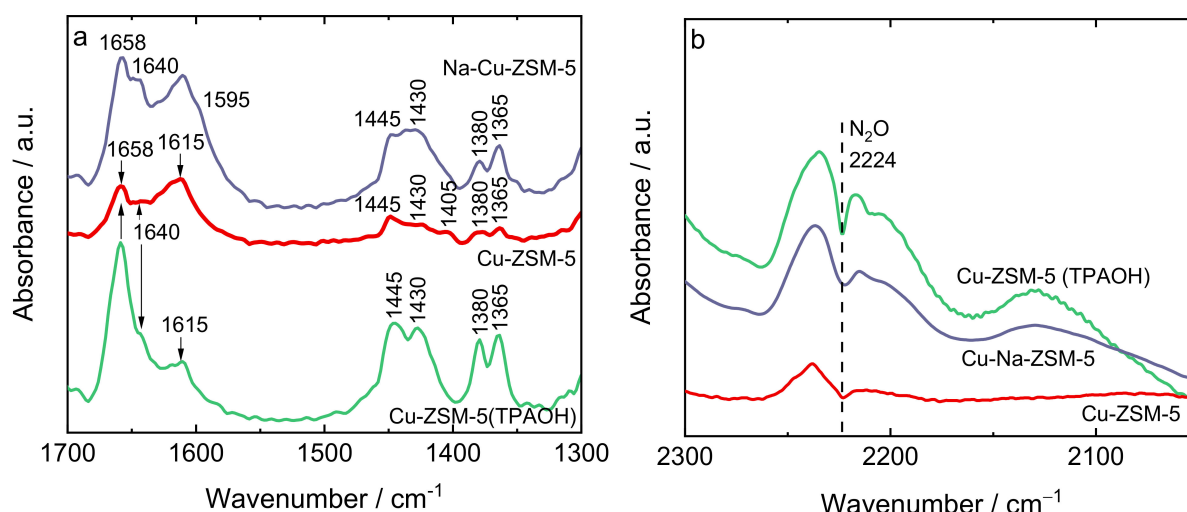


Figure 14. FT-IR difference spectra collected at 150°C after the adsorption NO , O_2 and NH_3 in the stoichiometric amounts ($c(\text{NO})/c(\text{O}_2)/c(\text{NH}_3) = 4:1:4$) on the Cu-exchanged ZSM-5 in the range of: (a) $1700\text{--}1300\text{ cm}^{-1}$ and (b) $2300\text{--}2050\text{ cm}^{-1}$.

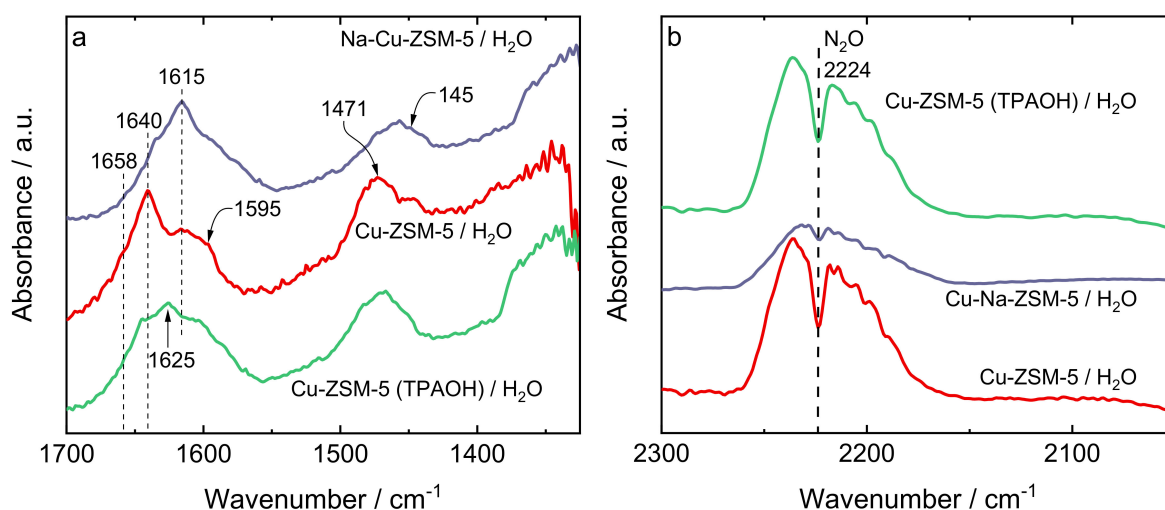


Figure 15. FT-IR difference spectra collected at 150 °C after the adsorption NO, O₂ and NH₃ in the stoichiometric amounts ($c(\text{NO})/c(\text{O}_2)/c(\text{NH}_3) = 4:1:4$) on the Cu-exchanged ZSM-5 in the presence of water vapor (5 vol.%) in the range of: (a) 1700–1325 cm⁻¹ and (b) 2300–2050 cm⁻¹.

3. Materials and Methods

3.1. Catalyst Preparation

The zeolites NH₄⁺-ZSM-5 ($n(\text{SiO}_2)/n(\text{Al}_2\text{O}_3) = 27$), used in this study, are commercially available from Clariant. H-ZSM-5 was obtained by the calcination (550 °C, 4 h, 1 °C min⁻¹) of the zeolite in its NH₄⁺-form.

NH₄⁺-ZSM-5 was treated with an aqueous solution of 0.2 M NaOH, TPAOH (tetrapropylammonium hydroxide) or a mixture of NaOH and TPAOH at 65 °C for 2 h under reflux (3 g of zeolite per 100 mL of solution). After treatment, the suspension was cooled down in an ice-bath, filtered and washed with distilled water until neutral pH. In the next step, the obtained material (besides the one treated with TPAOH) was transformed into the H-form by triple ion-exchange with 0.5 M NH₄NO₃ performed at 60 °C for 1 h. Finally, the resulting sample was again filtrated, washed, dried at room temperature and calcined (550 °C, 4 h, 1 °C min⁻¹).

H-ZSM-5 was subjected to ion-exchange with an aqueous solution of 0.05 M of co-cation precursor (NaNO₃) at 80 °C for 2 h (1 g of zeolite per 100 mL of solution).

The ZSM-5 samples were then ion-exchanged with an aqueous solution of copper (II) acetate (0.05 M) for 24 h at room temperature (1 g of zeolite per 100 mL of solution). Finally, the resulting Cu-exchanged sample was again filtered, washed, dried at room temperature and calcined (550 °C, 4 h, 1 °C min⁻¹).

The abbreviations of all samples and their preparation procedures are also presented in Table S2.

3.2. Catalyst Physico-Chemical Characterization

The XRD patterns were recorded using a HUBER G670 (Rimsting, Germany) diffractometer applying Cu-K_α radiation (wavelength: 0.154 nm). The samples were measured with a scanning range of the diffraction angle 2θ between 5° and 60° in intervals of 0.005°. X-ray powder patterns were used for structural identification of the relative crystallinity level (Cryst. level, Table 1) for all zeolites. Determination of the relative crystallinity was based on the intensity of the reflections in the range between 5–60°.

Analysis of Al, Si, Cu or Na content in the samples was carried out by inductively coupled plasma optical emission spectroscopy (ICP-OES) on Perkin Elmer, Optima 8000 instrument (Rodgau, Germany). The samples (ca. 20 mg) were digested in a mixture of HF (2 cm³, 47–51 wt %, Sigma-Aldrich), HNO₃ (3 cm³, 69 wt %, Sigma-Aldrich), and HCl (3 cm³, 35 wt %, Sigma-Aldrich) with microwave radiation (1 h, 200 °C). Before

measurement, HF was removed by microwave radiation (5 min, 200 °C) by complexing with H₃BO₃ (12 cm³, 99.99 wt %, Sigma-Aldrich).

Transmission electron microscopy (TEM) was carried out using a JEM-2100Plus instrument from JEOL (Tokyo, Japan) operating at an accelerating voltage of 200 kV. The images were taken with a 4K CMOS camera from TVIPS (Gauting, Germany). The TEM is equipped with a LaB₆ cathode and high-resolution pole piece to achieve a point resolution in TEM mode of 0.23 nm. The sample preparation was performed by grinding the sample in a mortar and pestle in ethanol, and the dispersed particles were supported on a Ni-TEM grid.

Nitrogen adsorption isotherms were recorded at −196 °C using a MicrotracBEL Corp., BELSORP-miniX (Haan/Duesseldorf, Germany). Before measurement, ca. 100–200 mg of the sample was activated at 250 °C and 1 Pa. The total pore volume was taken from the point $p/p_0 = 0.9857$. The specific surface area was calculated using the Brunauer–Emmett–Teller (BET) method and the pore width distribution was obtained using the Barret–Joyner–Halenda (BJH) method.

Diffuse Reflectance UV-Vis spectra of the samples were recorded at room temperature at Perkin Elmer Lambda 650S UV-Vis spectrometer (Rodgau, Germany) equipped with a 150 mm integrating sphere using Spectralon[®] (PTFE, reflective value 99%, Rodgau, Germany) as a reference. The experiments were carried out in the wavelength range of 200–900 nm with a step width of 1 nm and a slit width of 2 nm.

The EPR spectra were recorded at −196 °C with a Bruker ESP 300E spectrometer operating at a microwave frequency 9.5 GHz. The modulation amplitude and the microwave power were kept at 5 G and 2 mW, respectively. The spectra were simulated by using the Easyspin software (version 6.0.0-dev.26, University of Washington, Seattle, WA, USA) [46]. An axial spin Hamiltonian model was used for the simulation of each spectrum with a Lorentzian line shape and an equal line width for all the species. The dehydrated samples were obtained by placing about 3–20 mg of Cu-ZSM-5 into a 4 mm cell tube connected to a vacuum line and dehydrated under dynamic vacuum at 200 °C for 1 h, reaching a final pressure of 10^{−3} mbar.

TPD-NO_x profiles of the samples were recorded with a NO_x analyzer Eco Physics Inc., CLD 70S ECO Physics (Ann Arbor, MI, USA). Before the NO adsorption the sample (100 mg) placed in a fixed-bed flow microreactor (i.d., 6 mm; l., 300 mm) was outgassed in a flow of pure helium (20 mL min^{−1}) at 350 °C for 1 h. Subsequently, the microreactor was cooled down to 100 °C. The sample was saturated with 500 ppm of NO diluted in He (1 h, 120 mL min^{−1}) then was purged in a flow of 4 vol.% of O₂ diluted in He until a constant baseline level was reached (1.5 h, 50 mL min^{−1}). For the desorption step, the microreactor temperature was raised to 450 °C with a linear heating rate of 10 °C min^{−1} in a flow of 4 vol.% of O₂ diluted in He (50 mL min^{−1}). Furthermore, the TPD-NO_x was carried out applying different feeds, such as 500 ppm NO/He, 500 ppm NO/4 vol.% O₂/He or 500 ppm NO/4 vol.% O₂/5 vol.% H₂O/He mixture up to initial level is restored. Every time a fresh sample was applied. Afterwards, the sample was purged in a flow of pure He until a constant baseline level was reached (1.5 h, 50 mL min^{−1}). The microreactor temperature was raised to 450 °C with a linear heating rate of 10 °C min^{−1} in a flow of pure He (50 mL min^{−1}) for the desorption step.

Before FT-IR measurements, all samples were pressed into self-supporting wafers (ca. 5 mg^{−1} cm²) and in situ thermally treated in a home-made quartz IR cell at 550 °C under oxygen atmosphere (200 mbar) for 1 h. Upon these time the gaseous phase was evacuated for 10 min at the same temperature and the samples were cooled down to the pyridine (Avantor, Gliwice, Poland) or CO (Linde Gas, Poland, 99.5 vol.%) adsorption temperature. The acidic feature assessment was performed in quantitative experiments using pyridine (Py) as a probe. The measurements were realized by saturation of all acid sites in the catalysts with at 170 °C. Subsequently, physisorbed pyridine molecules were removed by 20 min evacuation at the same temperature. The concentrations of both Brønsted and Lewis acid sites were calculated from PyH⁺ and Py-L bands' maximum intensities by

using the respective values of the absorption coefficients. The redox copper sites speciation was assessed with CO adsorption in quantitative FT-IR studies. The concentration of Cu(I) species was assessed from maximum intensity of 2157 cm^{-1} band of $\text{Cu}^+(\text{CO})$ monocarbonyls recorded at room temperature. The Cu(II) concentration was determined from the maximum intensities of $\text{Cu}^{2+}_{\text{oxo}}(\text{CO})$ and $\text{Cu}^{2+}_{\text{exch}}(\text{CO})$ monocarbonyls formed by the ligation of CO to copper(II) sites at $-100\text{ }^\circ\text{C}$. All the FT-IR spectra (100 scans) were recorded with a Bruker Vertex 70 spectrometer equipped with an MCT detector. The spectral resolution was 2 cm^{-1} .

Time-resolved IR measurements of NO, O₂, NH₃ and H₂O mixture were carried out under flow conditions. Before the studies the catalysts were thermally treated in nitrogen flow at 400 $^\circ\text{C}$ for 1 h. After cooling to room temperature, the mixtures of $c(\text{NO})/c(\text{O}_2)/c(\text{NH}_3) = 4:1:4$ (and 5 vol.% H₂O when added) were passed through the catalysts. Then the IR cell was started to be heated up to 150 $^\circ\text{C}$ what was followed by spectra gathering. In this work the FT-IR spectra collected upon the contact of reagent mixture with the catalysts at 150 $^\circ\text{C}$ for 10 min are presented as the most representative for the surface species formed during NH₃-SCR. Difference spectra are presented, i.e., the spectrum of the activated zeolite was subtracted from the spectrum collected after the reactant' reaction. All the infrared spectral acquisitions were performed in transmission mode.

3.3. Catalytic Tests

The catalytic experiments were carried out in a fixed-bed quartz tube reactor (inner diameter: 6 mm, length: 200 mm). For catalytic experiments, a fraction of particle size in the range of 200–400 μm was used. Before each experiment, the catalysts (200 mg) were activated at 350 $^\circ\text{C}$ for 1.5 h under a flow of 50 mL min^{-1} of He and then cooled down to 50 $^\circ\text{C}$. After that, the simulated flue gas, with a total flow rate of 120 mL min^{-1} composed of 500 ppm NO, 575 ppm NH₃ and 4 vol.% O₂ and balance He, was switched on to pass through the catalyst bed. For selected samples, the catalytic tests were carried out in the presence of water vapor (5 vol.%). The gas hourly space velocity (GHSV) was determined to be $\sim 30,000\text{ h}^{-1}$. The reaction was carried out at atmospheric pressure and in a range of temperatures from 50 to 450 $^\circ\text{C}$ with an interval of 25–50 $^\circ\text{C}$. At each temperature, the reaction was stabilized for 70 min before the quantitative analysis of NO and N₂O concentration, the equilibration time to reach the steady-state was also proved to be appropriate according to the modeling results (Figure S3). The gas leaving the reactor was washed in a gas-washing bottle filled with concentrated phosphoric acid. The NO_x-converter was used to reduce NO₂ to NO, to measure the total concentration of NO_x. Analysis of the NO and N₂O was performed using a non-dispersive infrared sensor (NDIR) URAS 10E Fa. Hartmann und Braun (Frankfurt am Main, Germany).

The conversion of NO (X_{NO}) was determined according to Equation (1):

$$X_{\text{NO}} = [C_{\text{NO}}(z = 0) - C_{\text{NO}}(z = L)] / C_{\text{NO}}(z = 0) \times 100\% \quad (1)$$

where: $C_{\text{NO}}(z = 0)$ and $C_{\text{NO}}(z = L)$ represent the concentration of gaseous NO in the inlet (position of dimension z equals 0) and the outlet (position z equals the length of the bed L), respectively.

The yield of N₂O ($Y_{\text{N}_2\text{O}}$) was calculated according to Equation (2):

$$Y_{\text{N}_2\text{O}} = 2 \times C_{\text{N}_2\text{O}}(z = L) / [C_{\text{NO}}(z = 0) + C_{\text{NH}_3}(z = 0)] \times 100\% \quad (2)$$

where: $C_{\text{N}_2\text{O}}(z = L)$, $C_{\text{NO}}(z = 0)$ and $C_{\text{NH}_3}(z = 0)$ represent the concentration of N₂O in the outlet gas and the concentrations of NO and NH₃ in the inlet gas, respectively. Conversion and yield, both experimental and modeled were calculated according to Equations (1) and (2) after the steady-state was reached either experimentally or in silico. The experimental uncertainty of the calculated conversion was found to be $\pm 2\%$ as indicated by repeated measurements of identical catalysts.

3.4. Microkinetic Model

The microkinetic model describes the concentration of gaseous phase and coverage of the catalyst surface sites throughout the fixed-bed reactor as a function of (residence) time. Both non-isothermal TPD and isothermal catalytic activity experiments were investigated in the dynamic (transient) regime, specifically as a function of time and catalyst bed length. The model accounted the following phenomena: axial convection in gas through the void space in the catalytic bed, axial diffusion in the gas phase, adsorption and desorption kinetics, and the kinetics of surface reactions.

The rate of adsorption (r_j^{ads}) for adsorbate j (J is their number) at any time step or axial coordinate increment depends on the adsorption rate constant (k_j^{ads}), the concentration of the adsorbate in the gas phase (C_j), and a fraction of the vacant surface sites (θ_{VS}) (Equation (3)).

$$r_j^{ads} = k_j^{ads} \cdot C_j \cdot \theta_{VS} \quad (3)$$

Similarly, the rate of desorption (r_j^{des}) of the compound j depends on the desorption rate constant (k_j^{des}), and its surface coverage (Equation (4)).

$$r_j^{des} = k_j^{des} \cdot \theta_j \quad (4)$$

The surface reaction rate (r_i^{surf}) of the reaction i (I is their number) depends on the surface rate constant (k_i^{surf}) and the product of surface coverages of the rate-determining reactant(s) relevant for the reaction i (Equation (5)).

$$r_i^{surf} = TOF_i = k_i^{surf} \cdot \prod_{\in i} \theta_{j1} \quad (5)$$

As r_i^{surf} stands for the surface reaction rate per site, it directly represents the turn-over frequency (TOF_i) of the reaction and can be calculated at any t and z . For comparative purposes, the TOF was calculated for each reaction after the steady-state was reached and for the first catalyst layer in the bed, where the concentration of reactants (end hence TOF) was the highest (see Figure S3).

Alternatively, the reaction can also take place between the adsorbed reactants and a reactant from the gas phase. In this case, the rate equation is formulated as follows (Equation (6)).

$$r_i^{surf} = TOF_i = k_i^{surf} \cdot \theta_{j1} \cdot C_{j2} \quad (6)$$

Desorption and surface reaction rate constants were considered temperature-dependent according to the Arrhenius law. The temperature dependency of the rate constants was formulated according to the modified Arrhenius equation to avoid the mutual dependence of the frequency factor and activation energy (eventually causing local objective function minimum pits during the regression analysis) (Equations (7) and (8)).

$$k_i^{des}(T) = k_i^{des}(T_{ref}) \cdot \exp\left(\frac{Ea_i^{des}}{R} \left(\frac{1}{T_{ref}} - \frac{1}{T}\right)\right) \quad (7)$$

$$k_i^{surf}(T) = k_i^{surf}(T_{ref}) \cdot \exp\left(\frac{Ea_i^{surf}}{R} \left(\frac{1}{T_{ref}} - \frac{1}{T}\right)\right) \quad (8)$$

If required, the pre-exponential (frequency) factor (A_i^{surf}) is calculated as follows (Equation (9)).

$$A_i^{surf} = k_i^{surf}(T_{ref}) \cdot \exp\left(\frac{Ea_i^{surf}}{R T_{ref}}\right) \quad (9)$$

Molar balances for gas concentrations (C_j) involve the contribution of convective (v_z stands for the linear velocity of fluid) and diffusive flux (D_j^e stands for the effective diffusivity of the compound j) [47] in the axial direction (z), as well as the rate of adsorption and desorption, the latter is compensated with the capacity of the gas phase (V^G is the volume of the void in the bed) and the catalyst surface (n_{TS} is the total amount of surface sites available in the bed). Radial flux was neglected, due to the highly porous bed of small particles that acted as a static mixer and resulted in uniform gas concentration in the radial dimension (Equation (10)).

$$\frac{\partial C_j}{\partial t} = -\frac{\partial}{\partial z} \left[v_z \cdot C_j - D_j^e \frac{\partial C_j}{\partial z} \right] - r_j^{ads} + r_j^{des} \frac{n_{TS}}{V^G} \quad (10)$$

The total amount of surface sites depends on the surface sites density (q_{tot}) and the mass of the catalyst placed in the reactor (Equation (11)).

$$n_{TS} = q_{tot} \cdot m_{cat} \quad (11)$$

The volume of the void (V^G) depends on the bed porosity (α) and the total volume of the tube (V) where the catalyst is embedded (Equation (12)).

$$V^G = V \cdot \alpha \quad (12)$$

Linear velocity (v_z) in the catalytic bed depends on the set volumetric flow (\dot{V}) at ambient temperature (T_{MFC}), bed porosity, tube cross-sectional area and the temperature in the reactor (T) (Equation (13)). Relevant parameters are collected in Table S3.

$$v_z(T) = \frac{4\dot{V}}{\alpha \pi D^2} \left(\frac{T}{T_{MFC}} \right) \quad (13)$$

The balances for surface coverages depend on the adsorption and desorption rates, as well as the surface rates of the corresponding reactions (i) converting or yielding j at given t and z (Equation (14)).

$$\frac{\partial \theta_j}{\partial t} = r_j^{ads} \frac{V^G}{n_{TS}} + r_j^{des} + \sum_i \pm r_i^{surf} \quad (14)$$

The balance for vacant sites accounts for all adsorption and desorption rates as well as the surface rates of the eventual reactions with non-stoichiometric reactions regarding the surface reactants consumed and products formed (Equation (15)).

$$\frac{\partial \theta_{VS}}{\partial t} = -\sum_j r_j^{ads} \frac{V^G}{n_{TS}} + \sum_j r_j^{des} + \sum_i \pm r_i^{surf} \quad (15)$$

A system of partial differential equations (PDE) was formulated according to the molar balances for the components in the gas phase and on the catalyst surface in at every increment of the packed bed length (z from 0 to Z) and at any time increment (t from 0 to t_{end}). The system of PDE was solved numerically in MATLAB 2018a software. To optimize the computation time, the PDE were transformed into a system of ordinary differential equations (ODE). The concentration and surface coverages of all compounds were hence formulated at each z position and solved as a function of time with ODE 23tb solver based on the implicit Runge-Kutta formula. Specifically, 6 PDEs (for three gas concentrations and 3 surface coverages) were transferred into 600 ODEs to calculate their value at 100 z locations $\{z \mid 0 \leq z \leq L\}$ throughout the catalyst bed for each time increment (approximately 1000 in total) until the steady-state (NH_3 -SCR test) or complete desorption (TPD- NO_x test) was reached. For the simulation of NH_3 -SCR and TPD- NO_x the same model was used but utilizing different initial and boundary conditions, specifically by setting coverage of sites as completely vacant (SCR) or saturated (TPD) at $t = 0$ and by

setting the actual inlet gas concentration throughout the simulation (without NH₃ and NO during TPD tests).

Activation energies and rate constants at reference temperature were the parameters optimized during the regression analysis. The objective function was minimized using the Nelder–Mead algorithm, while the Levenberg–Marquardt algorithm was used for the determination of 95% confidence intervals (Equation (16)).

$$f(Ea_i^{surf}, Ea_j^{des}, k_j^{ads}, k_i^{surf}, k_j^{des}) = \sum_j (C_j^{meas} - C_j^{calc}(Ea_i^{surf}, Ea_j^{des}, k_j^{ads}, k_i^{surf}, k_j^{des}))^2 \quad (16)$$

4. Conclusions

We have studied the effect of textural properties and co-cation (Na⁺) of the resulting Cu-exchanged zeolites in the selective catalytic reduction of NO_x with NH₃ (NH₃-SCR). The micro-/mesoporous materials were obtained in the post-synthetic modification of H-ZSM-5 in an aqueous solution of NaOH, TPAOH or NaOH/TPAOH. The post-synthetic modification of TPAOH did not cause the creation of mesoporosity in H-ZSM-5. Cu-ZSM-5 revealed the highest activity and selectivity among all tested catalysts, both in the absence and presence of H₂O. Thus, the results of the catalytic data revealed that the microporous structure was necessary for the formation of isolated Cu⁺/Cu²⁺. At the same time, the presence of the co-cations led to the formation of aggregated copper species, i.e., [Cu–O–Cu]²⁺. The aggregated copper species ([Cu–O–Cu]²⁺ and CuO_x) present in Cu-ZSM-5 (TPAOH) led to the NH₃ oxidation at higher temperatures (above 350–400 °C). The presence of H₂O has a positive effect on the selectivity of NH₃-SCR, as it reduces the reaction rate constants (and TOF) of parallel NH₃ oxidation reaction by the order of magnitude for all the catalysts tested.

Supplementary Materials: The following are available online at <https://www.mdpi.com/article/10.3390/catal11070843/s1>, Table S1: Calculated parameters for adsorption and desorption kinetics, Table S2: Preparation procedures applied for modifications of parent ZSM-5, Table S3: Relevant parameters for kinetic modelling, Figure S1: a) NO concentration in the gas phase and b) NO surface coverage as a function of time on stream and position in the reactor during the TPD-NO_x at 150 °C over Na-Cu-ZSM-5 conversion (conditions: 0.1 g of catalyst, 50 ml min⁻¹, 0 ppm NO, heat-up rate 10 K min⁻¹, initial temperature 50 °C), Figure S2: Experimental cw-EPR spectra of a) hydrated and b) dehydrated Cu-ZSM-5 acquired at room temperature, Figure S3: TOF₁ as a function of time on stream and position in the reactor for NH₃-SCR at 150 °C over Cu-ZSM-5 conversion in a) absence and b) presence of 5 vol.-% H₂O (conditions: 0.2 g of catalyst, 120 mL min⁻¹, 500 ppm NO, 575 ppm NH₃).

Author Contributions: M.J., Conceptualization, Methodology, Investigation, Data Curation, Writing—Original Draft, Writing—Review and Editing; K.G.-M., Investigation, Data Curation, Writing—Review and Editing; M.G., Investigation, Data Curation, Writing—Review and Editing; P.C.B., Investigation, Data Curation, Writing—Review and Editing; D.P., Investigation, Data Curation; K.P., Investigation, Data Curation; M.L., Data Curation; A.P., Review; B.L., Review; R.G., Review. All authors have read and agreed to the published version of the manuscript.

Funding: K.G.M. acknowledges the Grant No. 2015/18/E/ST4/00191 from the National Science Centre, Poland. M.G. & B.L. acknowledge the financial support by the Slovenian Research Agency (Core Funding P2-0152). P.C.B. & A.P. acknowledge the funding from the European Union's Horizon 2020 research and innovation program under the Marie Skłodowska-Curie Grant Agreement No. 813209 (PARACAT).

Institutional Review Board Statement: Not applicable.

Informed Consent Statement: Not applicable.

Data Availability Statement: Not applicable.

Acknowledgments: We acknowledge support from the German Research Foundation (DFG) and Leipzig University within the program of Open Access Publishing. P.C.B. acknowledges Mario Chiesa for the utilization of the EPR at the University of Turin.

Conflicts of Interest: The authors declare no conflict of interest.

References

1. Deka, U.; Lezcano-Gonzalez, I.; Weckhuysen, B.M.; Beale, A.M. Local environment and nature of Cu active sites in zeolite-based catalysts for the selective catalytic reduction of NO_x. *ACS Catal.* **2013**, *3*, 413–427. [\[CrossRef\]](#)
2. Tarach, K.A.; Jabłońska, M.; Pyra, K.; Liebau, M.; Reiprich, B.; Gläser, R.; Góra-Marek, K. Effect of zeolite topology on NH₃-SCR activity and stability of Cu-exchanged zeolites. *Appl. Catal. B Environ.* **2020**, *284*, 119752. [\[CrossRef\]](#)
3. Rutkowska, M.; Pacia, I.; Baskag, S.; Kowalczyk, A.; Piwowarska, Z.; Duda Michałand Tarach, K.A.; Góra-Marek, K.; Michalik, M.; Diaz, U.; Chmielarz, L. Catalytic performance of commercial Cu-ZSM-5 zeolite modified by desilication in NH₃-SCR and NH₃-SCO processes. *Microporous Mesoporous Mater.* **2017**, *246*, 193–206. [\[CrossRef\]](#)
4. Sultana, A.; Nanba, T.; Haneda, M.; Sasaki, M.; Hamada, H. Influence of co-cations on the formation of Cu⁺ species in Cu/ZSM-5 and its effect on selective catalytic reduction of NO_x with NH₃. *Appl. Catal. B Environ.* **2010**, *101*, 61–67. [\[CrossRef\]](#)
5. Peng, C.; Yan, R.; Peng, H.; Mi, Y.; Liang, J.; Liu, W.; Wang, X.; Song, G.; Wu, P.; Liu, F. One-pot synthesis of layered mesoporous ZSM-5 plus Cu ion-exchange: Enhanced NH₃-SCR performance on Cu-ZSM-5 with hierarchical pore structures. *J. Hazard. Mater.* **2020**, *385*, 121593. [\[CrossRef\]](#) [\[PubMed\]](#)
6. Gao, F.; Wang, Y.; Washton, N.M.; Kollar, M.; Szanyi, J.; Peden, C.H.F. Effects of alkali and alkaline earth cations on the activity and hydrothermal stability of Cu/SSZ-13 NH₃-SCR catalysts. *ACS Catal.* **2015**, *5*, 6780–6791. [\[CrossRef\]](#)
7. Zhao, Z.; Yu, R.; Zhao, R.; Shi, C.; Gies, H.; Xiao, F.-S.; De Vos, D.; Yokoi, T.; Bao, X.; Kolb, U.; et al. Cu-exchanged Al-rich SSZ-13 zeolite from organotemplate-free synthesis as NH₃-SCR catalyst: Effects of Na⁺ ions on the activity and hydrothermal stability. *Appl. Catal. B Environ.* **2017**, *217*, 421–428. [\[CrossRef\]](#)
8. Delahay, G.; Ayala Villagomez, E.; Ducere, J.-M.; Berthomieu, D.; Goursot, A.; Coq, B. Selective catalytic reduction of NO by NH₃ on Cu-faujasite catalysts: An experimental and quantum chemical approach. *Chem. Phys. Chem.* **2002**, *3*, 686–692. [\[CrossRef\]](#)
9. Kieger, S.; Delahay, G.; Coq, B. Influence of co-cations in the selective catalytic reduction of NO by NH₃ over copper exchanged faujasite zeolites. *Appl. Catal. B Environ.* **2000**, *25*, 1–9. [\[CrossRef\]](#)
10. Coq, B.; Delahay, G.; Durand, R.; Berthomieu, D.; Ayala-Villagomez, E. The influence of cocations H, Na, and Ba on the properties of Cu-faujasite for the selective catalytic reduction of NO by NH₃: An O perando DRIFT study. *J. Phys. Chem. B* **2004**, *108*, 11062–11068. [\[CrossRef\]](#)
11. Kučera, J.; Nachtigall, P.; Kotrla, J.; Košová, G.; Čejka, J. Pyrrole as a probe molecule for characterization of basic sites in ZSM-5: A combined FTIR spectroscopy and computational study. *J. Phys. Chem. B* **2004**, *108*, 16012–16022. [\[CrossRef\]](#)
12. Roth, W. Cation size effects in swelling of the layered zeolite precursor MCM-22-P. *Pol. J. Chem.* **2006**, *80*, 703–708.
13. Ensor, D.D.; Anderson, H.L.; Conally, T.G. Heats of mixing and heats of dilution of tetrapropylammonium chloride. Temperature dependence. *J. Phys. Chem.* **1974**, *78*, 77–80. [\[CrossRef\]](#)
14. Helmkamp, M.M.; Davis, M.E. Synthesis of porous silicates. *Annu. Rev. Mater. Sci.* **1995**, *25*, 161–192. [\[CrossRef\]](#)
15. King, D.L.; Faz, C. Desulfurization of Tier 2 gasoline by divalent copper-exchanged zeolite Y. *Appl. Catal. A Gen.* **2006**, *311*, 58–65. [\[CrossRef\]](#)
16. Sárkány, J.; d'Itri, J.L.; Sachtler, W.M.H. Redox chemistry in excessively ion-exchanged Cu/Na-ZSM-5. *Catal. Lett.* **1992**, *16*, 241–249. [\[CrossRef\]](#)
17. Zhang, Y.; Leo, K.M.; Sarofim, A.F.; Hu, Z.; Flytzani-Stephanopoulos, M. Preparation effects on the activity of Cu-ZSM-5 catalysts for NO decomposition. *Catal. Lett.* **1995**, *31*, 75–89. [\[CrossRef\]](#)
18. Thommes, M.; Kaneko, K.; Neimark, A.V.; Olivier, J.P.; Rodriguez-Reinoso, F.; Rouquerol, J.; Sing, K.S.W. Physisorption of gases, with special reference to the evaluation of surface area and pore size distribution (IUPAC Technical Report). *Pure Appl. Chem.* **2015**, *87*, 1051–1069. [\[CrossRef\]](#)
19. Mei, C.; Wen, P.; Liu, Z.; Liu, H.; Wang, Y.; Yang, W.; Xie, Z.; Hua, W.; Gao, Z. Selective production of propylene from methanol: Mesoporosity development in high silica HZSM-5. *J. Catal.* **2008**, *258*, 243–249. [\[CrossRef\]](#)
20. Groen, J.C.; Moulijn, J.A.; Pérez-Ramirez, J. Alkaline posttreatment of MFI zeolites. From accelerated screening to scale-up. *Ind. Eng. Chem. Res.* **2007**, *46*, 4193–4201. [\[CrossRef\]](#)
21. Góra-Marek, K.; Brylewska, K.; Tarach, K.A.; Rutkowska, M.; Jabłońska, M.; Choi, M.; Chmielarz, L. IR studies of Fe modified ZSM-5 zeolites of diverse mesopore topologies in the terms of their catalytic performance in NH₃-SCR and NH₃-SCO processes. *Appl. Catal. B Environ.* **2015**, *179*, 589–598. [\[CrossRef\]](#)
22. Abello, S.; Bonilla, A.; Perez-Ramirez, J. Mesoporous ZSM-5 zeolite catalysts prepared by desilication with organic hydroxides and comparison with NaOH leaching. *Appl. Catal. A Gen.* **2009**, *364*, 191–198. [\[CrossRef\]](#)
23. Chen, B.-H.; Chao, Z.-S.; He, H.; Huang, C.; Liu, Y.-J.; Yi, W.-J.; Wei, X.-L.; An, J.-F. Towards a full understanding of the nature of Ni (II) species and hydroxyl groups over highly siliceous HZSM-5 zeolite supported nickel catalysts prepared by a deposition-precipitation method. *Dalt. Trans.* **2016**, *45*, 2720–2739. [\[CrossRef\]](#)
24. Huo, Q.; Margolese, D.I.; Stucky, G.D. Surfactant control of phases in the synthesis of mesoporous silica-based materials. *Chem. Mater.* **1996**, *8*, 1147–1160. [\[CrossRef\]](#)
25. Martins, L.; Peguin, R.P.S.; Wallau, M.; González, E.A.U. Cu-, Co-, Cu/Ca- and Co/Ca-exchanged ZSM-5 zeolites: Activity in the reduction of NO with methane or propane. In *Studies in Surface Science and Catalysis*; Elsevier: Amsterdam, The Netherlands, 2004; Volume 154, pp. 2475–2483.

26. Palčić, A.; Bruzzese, P.C.; Pyra, K.; Bertmer, M.; Góra-Marek, K.; Poppitz, D.; Pöpl, A.; Gläser, R.; Jabłońska, M. Nanosized Cu-SSZ-13 and its application in NH₃-SCR. *Catalysts* **2020**, *10*, 506. [[CrossRef](#)]
27. Olsson, L.; Sjövall, H.; Blint, R.J. Detailed kinetic modeling of NO_x adsorption and NO oxidation over Cu-ZSM-5. *Appl. Catal. B Environ.* **2009**, *87*, 200–210. [[CrossRef](#)]
28. Lee, D.K. Quantification and redox property of the oxygen-bridged Cu²⁺ dimers as the active sites for the NO decomposition over Cu-ZSM-5 catalysts. *Korean J. Chem. Eng.* **2004**, *21*, 611–620. [[CrossRef](#)]
29. Torre-Abreu, C.; Ribeiro, M.F.; Henriques, C.; Delahay, G. Characterisation of CuMFI catalysts by temperature programmed desorption of NO and temperature programmed reduction. Effect of the zeolite Si/Al ratio and copper loading. *Appl. Catal. B Environ.* **1997**, *12*, 249–262. [[CrossRef](#)]
30. Modén, B.; Da Costa, P.; Fonfó, B.; Lee, D.K.; Iglesia, E.; Lee, D.K. Kinetics and mechanism of steady-state catalytic NO decomposition reactions on Cu-ZSM5. *J. Catal.* **2002**, *209*, 75–86. [[CrossRef](#)]
31. Zhang, W.X.; Yahiro, H.; Mizuno, N.; Iwamoto, M.; Izumi, J. Silver ion-exchanged zeolites as highly effective adsorbents for removal of NO_x by pressure swing adsorption. *J. Mater. Sci. Lett.* **1993**, *12*, 1197–1198. [[CrossRef](#)]
32. Torre-Abreu, C.; Ribeiro, M.F.; Henriques, C.; Delahay, G. NO TPD and H₂-TPR studies for characterisation of CuMOR catalysts The role of Si/Al ratio, copper content and cocation. *Appl. Catal. B Environ.* **1997**, *14*, 261–272. [[CrossRef](#)]
33. Landi, G.; Lisi, L.; Pirone, R.; Russo, G.; Tortorelli, M. Effect of water on NO adsorption over Cu-ZSM-5 based catalysts. *Catal. Today* **2012**, *191*, 138–141. [[CrossRef](#)]
34. Schoonheydt, R.A. Transition metal ions in zeolites: Siting and energetics of Cu²⁺. *Catal. Rev. Eng.* **1993**, *35*, 129–168. [[CrossRef](#)]
35. Smeets, P.J.; Groothaert, M.H.; Schoonheydt, R.A. Cu based zeolites: A UV—Vis study of the active site in the selective methane oxidation at low temperatures. *Catal. Today* **2005**, *110*, 303–309. [[CrossRef](#)]
36. Dedecek, J.; Sobalik, Z.; Tvaruzkova, Z.; Kaucy, D.; Wichterlova, B. Coordination of Cu ions in high-silica zeolite matrixes. Cu+ photoluminescence, IR of NO adsorbed on Cu²⁺, and Cu²⁺ ESR study. *J. Phys. Chem.* **1995**, *99*, 16327–16337. [[CrossRef](#)]
37. Fernández, E.; Moreno-González, M.; Moliner, M.; Blasco, T.; Boronat, M.; Corma, A. Modeling of EPR parameters for Cu (II): Application to the selective reduction of NO_x catalyzed by Cu-zeolites. *Top. Catal.* **2018**, *61*, 810–832. [[CrossRef](#)]
38. Anderson, M.W.; Kevan, L. Study of copper(2+)-doped zeolite NaH-ZSM-5 by electron spin resonance and electron spin echo modulation spectroscopies. *J. Phys. Chem.* **1987**, *91*, 4174–4179. [[CrossRef](#)]
39. Conesa, J.C.; Soria, J. Electron spin resonance of copper-exchanged Y zeolites. Part 1—Behaviour of the cation during dehydration. *J. Chem. Soc. Faraday Trans. 1 Phys. Chem. Condens. Phases* **1979**, *75*, 406–422. [[CrossRef](#)]
40. Oliva, C.; Selli, E.; Ponti, A.; Correale, L.; Solinas, V.; Rombi, E.; Monaci, R.; Forni, L. FTIR and EPR characterisation of copper-exchanged mordenites and beta zeolites. *J. Chem. Soc. Faraday Trans.* **1997**, *93*, 2603–2608. [[CrossRef](#)]
41. Carl, P.J.; Larsen, S.C. Variable-temperature electron paramagnetic resonance studies of copper-exchanged zeolites. *J. Catal.* **1999**, *182*, 208–218. [[CrossRef](#)]
42. Kucherov, A.V.; Karge, H.G.; Schlögl, R. Quantitative ESR study of the CuH-ZSM-5 system: Influence of preparation and pretreatment techniques on the valence state of copper. *Microporous Mesoporous Mater.* **1998**, *25*, 7–14. [[CrossRef](#)]
43. Groothaert, M.H.; Pierloot, K.; Delabie, A.; Schoonheydt, R.A. Identification of Cu (ii) coordination structures in Cu-ZSM-5, based on a DFT/ab initio assignment of the EPR spectra. *Phys. Chem. Chem. Phys.* **2003**, *5*, 2135–2144. [[CrossRef](#)]
44. Góra-Marek, K.; Palomares, A.E.; Glanowska, A.; Sadowska, K.; Datka, J. Copper sites in zeolites—quantitative IR studies. *Microporous Mesoporous Mater.* **2012**, *162*, 175–180. [[CrossRef](#)]
45. Sjövall, H.; Olsson, L.; Fridell, E.; Blint, R.J. Selective catalytic reduction of NO_x with NH₃ over Cu-ZSM-5—The effect of changing the gas composition. *Appl. Catal. B Environ.* **2006**, *64*, 180–188. [[CrossRef](#)]
46. Stoll, S.; Schweiger, A. EasySpin, a comprehensive software package for spectral simulation and analysis in EPR. *J. Magn. Reson.* **2006**, *178*, 42–55. [[CrossRef](#)] [[PubMed](#)]
47. Fairbanks, D.F.; Wilke, C.R. Diffusion coefficients in multicomponent gas mixtures. *Ind. Eng. Chem.* **1950**, *42*, 471–475. [[CrossRef](#)]